

Contents lists available at ScienceDirect

# Journal of Experimental Marine Biology and Ecology

journal homepage: www.elsevier.com/locate/jembe





# Seasonality of bioirrigation by the maldanid polychaete *Clymenella torquata* and related oxygen dynamics in permeable sediments

Ian P. Dwyer<sup>a</sup>, Darci A. Swenson Perger<sup>a</sup>, Molly Graffam<sup>a,b</sup>, Robert C. Aller<sup>a</sup>, Laura M. Wehrmann<sup>a</sup>, Nils Volkenborn<sup>a,\*</sup>

- <sup>a</sup> School of Marine and Atmospheric Sciences, Stony Brook University, Stony Brook, NY 11794-5000, USA
- b Cornell Cooperative Extension Suffolk County, Extension Education Center, 423 Griffing Avenue, Suite 100, Riverhead, NY 11901-3071, USA

#### ARTICLE INFO

Keywords:
Bioturbation
Permeable sediments
Oxygen dynamics
Clymenella torquata
Biogeochemistry
Seasonality

#### ABSTRACT

Benthic organisms in coastal sediments affect elemental cycling and control benthic-pelagic coupling through particle reworking and ventilation of their burrows. Bioirrigation and associated porewater advection create intermittently oxic regions within sediments. The spatio-temporal patterns of such biogenic redox oscillations likely respond to seasonal factors, but quantitative information on the seasonality of bioirrigator behaviors and associated redox dynamics is scarce. We examined bioirrigation by the maldanid polychaete Clymenella torquata and its impacts on sediment oxygenation patterns in permeable sediments using high-resolution planar optode oxygen imaging. In sediment mesocosms with reconstructed summer-collected sediment, the durations of pumping and resting varied inversely with temperature. The average durations of pumping and resting increased from 4 min/4 min at 21 °C, to 6 min/6 min at 12 °C, to 15 min/14 min at 5 °C. In intact cores collected in summer, irrigation patterns (3.5 min/3.5 min) were similar to those observed at 21 °C during the temperature ramp. Pumping and resting durations in intact cores collected in winter at 6 °C averaged 9 min/26 min, significantly different from patterns at comparable temperatures in the temperature ramp. Pumping patterns strongly affected the temporal patterns of redox dynamics in surrounding sediments. In addition, temperature strongly affected burrow irrigation depth (exclusively within the top  $\sim$ 10 cm at 21 °C, and down to  $\sim$ 20 cm at 5-6 °C with an apparent transition at  $\sim 15$  °C), indicating that the zone with dynamic redox conditions migrates vertically on a seasonal basis. The differences in pumping patterns between in- and out-of-season experiments and the effect of temperature on irrigation depth underscore the importance of conducting experiments with bioturbators in-season and at field temperatures. The observed seasonal differences in bioirrigation patterns and associated spatio-temporal redox dynamics suggest that rates and pathways of redox-sensitive diagenetic processes and benthic chemical fluxes in permeable sediments likely show considerable seasonal variation.

#### 1. Introduction

Coastal oceans only make up  $\sim$ 7.2% of the total ocean surface area but are disproportionately important in global biogeochemical cycles because of the close coupling between the seafloor, overlying water, and the atmosphere in these shallow water environments (Liu et al., 2010). For example, sediment-overlying water exchange is a critical component of the processes affecting coastal ocean  $\rm CO_2$  uptake, diagenetic redox reaction pathways, and carbon sequestration and storage (Thomas et al., 2009; Cai, 2011; Blair and Aller, 2012). The exchange of solutes between sediments and the overlying water column is significantly affected by

bioturbating organisms that establish and maintain burrows in otherwise anoxic sediments and ventilate them with oxic overlying water (Forster and Graf, 1995; Kristensen and Kostka, 2005; Volkenborn et al., 2016). Bioirrigation not only creates intermittently oxic conditions but also oxidized sediment regions in which the redox potential can be elevated beyond the duration of oxygen presence (Forster, 1996). Seasonal variations in the spatio-temporal patterns of oxygen supply to subsurface sediment and the resulting redox dynamics are not well constrained. This knowledge gap is problematic, as intermittently-oxic conditions affect net remineralization rates, microbial activity and community structure, and redox processes differently than continuous

E-mail addresses: ian.dwyer@stonybrook.edu (I.P. Dwyer), darci.swenson@stonybrook.edu (D.A. Swenson Perger), meg372@cornell.edu (M. Graffam), robert. aller@stonybrook.edu (R.C. Aller), laura.wehrmann@stonybrook.edu (L.M. Wehrmann), nils.volkenborn@stonybrook.edu (N. Volkenborn).

<sup>\*</sup> Corresponding author.

conditions, and the frequency and duration of oxic events is likely an important determinant of rates and signatures of benthic fluxes (Aller, 1994; Volkenborn et al., 2010; Wehrmann et al., 2023).

The relative stability of redox conditions and time scaling of redox disturbances induced by bioturbating infauna may strongly control diagenetic pathways and subsequent fluxes into overlying water by diffusion and (bio-)advection. In the absence of bioturbation, oxygen is typically consumed in the uppermost few mm to cm of coastal sediments (Jørgensen and Revsbech, 1985), and organic carbon is oxidized by a range of remineralization processes, including ammonification, denitrification, dissimilatory manganese and iron reduction, and sulfate reduction (Burdige, 2011), leading to the production of dissolved constituents such as ammonium, nitrate, nitrite and N2, Mn2+, Fe2+, and H<sub>2</sub>S, respectively. However, many of these processes have multiple steps with intermediate products, often governed by second-order kinetics incorporating both time-dependence and concentration-dependence (Aller and Aller, 1998). While some of the end products are considered to be relatively stable, many intermediate products can be quite reactive, and the reactions are often reversible to some extent (Aller, 2014). For example, redox-active metastable minerals, while notable for their stability relative to other intermediate products of redox processes, will eventually react into fully oxidized or reduced end products if redox conditions remain constant (Peiffer et al., 2021). These minerals are particularly bioavailable, and their presence may enhance the rates of microbially-mediated redox reactions (Peiffer et al., 2021). Other intermediate products such as reactive oxygen species are extremely shortlived but capable of directly oxidizing organic matter and damaging microbes (Trusiak et al., 2018). The fate of N2O, which is formed during denitrification also likely depends on redox conditions (Hölker et al., 2015).

In the present study, we assessed the seasonality of bioirrigation activity patterns and sedimentary oxygen dynamics associated with bioturbation by the maldanid polychaete Clymenella torquata (Leidy, 1855), a prolific deposit feeder in permeable sediments. C. torquata is commonly found in intertidal and shallow subtidal sandflats along the North American East and Gulf coasts and has become invasive in the Pacific Northwest (Mangum, 1964; Mach et al., 2012). Other maldanid species are abundant in continental shelf and slope sediments (Levin et al., 1997). Maldanids are head-down, tube-building, deposit-feeding polychaetes (Dobbs and Whitlatch, 1982). They ingest sediment at depth and defecate at the sediment surface. Once a feeding void is formed, maldanids are also known to subduct organic-rich surface sediment with their posterior segments (Dobbs and Whitlatch, 1982; Levin et al., 1997). In the field, densities of this worm are often as high as 250–675 individuals/m<sup>2</sup> (sometimes as high as 150,000 individuals/m<sup>2</sup>) in their native range, and abundances up to 1680 individuals/m<sup>2</sup> have been reported in areas where they have become invasive (Mangum, 1964; Mach et al., 2012).

C. torquata is a pocket injection bioirrigator. It has a blind-ended burrow and pumps overlying water downward through sediment-lined tubes into unlined feeding pockets, resulting in the forced introduction of overlying water to permeable pore spaces and subsequent advective transport of porewater through the surrounding sediment and across the sediment-water interface (Meysman et al., 2006). Mangum (1964) measured C. torquata irrigation rates of ~2.14 mL/h/individual at 12.5 °C, with irrigation events occurring every 15-33 min with no apparent diurnal or tidal rhythms. These pumping events are thought to flush the burrow with overlying water (Mangum, 1964), but the geochemical expression of intermittent irrigation in terms of redox dynamics and the spatial scale of influence has not been studied. Furthermore, past experiments were performed with individual worms in confined sediment-filled glass tubes (1.2 cm inside diameter) and did not include an acclimation period to laboratory temperatures (Mangum, 1964). Mangum attempted to examine the effect of seasonality on irrigation patterns, but this attempt yielded insufficient data (Mangum, 1964).

Planar optode imaging of dissolved O<sub>2</sub> shows great promise in the quantitative study of both bioirrigator behavior and its effects (Polerecky et al., 2005; Polerecky et al., 2006). By allowing measurements of 2-dimensional dissolved O<sub>2</sub> profiles with sub-mm spatial resolution, submin temporal resolution, and µM precision under close to in-situ conditions, it can yield new insights into the O2 dynamics induced by animals throughout the bioturbated zone (Polerecky et al., 2005; Polerecky et al., 2006). From such high-resolution planar optode imaging data, it is possible to infer the activity patterns of animals from fluctuations in the O<sub>2</sub> that they introduce to the sediment during burrow irrigation, and it is further possible to derive fine-scale O2 dynamics such as oxygen consumption rates, oxic probability, oxic-anoxic oscillation frequency, and the lengths of oxic and anoxic events in specific areas of the sediment column (Polerecky et al., 2005; Polerecky et al., 2006; Matsui et al., 2011; Volkenborn et al., 2010; Volkenborn et al., 2012a; Volkenborn et al., 2012b; Volkenborn et al., 2016). Compared to traditional chemical profiling techniques, oxygen imaging offers the advantage of capturing both vertical and horizontal heterogeneity, both in a nearcontinuous fashion, which makes it ideal for studying bioturbated systems, in which pronounced spatial heterogeneity and temporal variability of redox conditions has been demonstrated (Forster, 1996).

In this study, high-resolution planar optode imaging was used to assess season-specific O2 concentration fields and oxygenation patterns within and around burrows of C. torquata inhabiting permeable muddy sand. Sediment oxygenation events were used to identify periods of active irrigation and resting as well as vertical distributions of animal acitivity. A series of oxygen imaging experiments were conducted using narrow "antfarm" aquaria containing sieved and reconstructed sediment with added maldanids as well as intact, naturally populated sediment cores. O2 consumption rates in sediments affected by ventilation events were estimated from the time-dependent O2 concentration decline following an oxygenation event. Calculations of oxic condition probability, redox oscillation frequency, and mean duration of oxygenation at a given location were made based on time-dependent O2 patterns. These data can inform future studies with bioirrigation mimics and mechanistic reaction-transport models that consider the kinetics of biogeochemical transformations and advective transport in bioturbated permeable sediments.

#### 2. Methods

#### 2.1. Laboratory experiments

We carried out three separate experiments between July 2015 and August 2020. Two approaches were used: individual or multiple maldanids added to sediment in narrow antfarm aquaria and cylindrical cores with intact sediment collected within a dense maldanid bed. Sediment and maldanids for all experiments were collected from the low intertidal of a sandflat near Old Ponquogue Bridge Marine Park, Hampton Bays, NY, USA (40.841589728685385 $^{\rm O}$  N, 72.49810072232744 $^{\rm O}$ W). The sediment at the site is a muddy sand with a permeability of  $\sim\!1.6\times10^{-11}$  m $^2$  (16.2 darcys), as determined by flow rates measured under multiple pressure heads, and a porosity of  $\sim\!0.44$ , as determined by dehydrating water-saturated samples.

# 2.1.1. Experimental set-ups

"Antfarm" aquaria consisted of a piece of tubing sandwiched between two rectangular plates of polycarbonate and held under tension by bolts to form a U-shaped seal enclosing a volume with a large width and height compared to its minimal thickness (dimensions varied and are provided for each individual experiment below, but thickness was always substantially larger than typical worm tube diameters of  $\sim 1-2$  mm). Front plates of aquaria were equipped with oxygen-sensitive foils (Precht et al., 2004) glued to the inside with double-sided adhesive film (X-film DX1). An example of this type of aquarium is shown in Supplementary Fig. 1A. For experiments in which antfarm aquaria were used,

sediment was collected with cores to a depth of  $\sim 30$  cm, separating the upper 2 cm of sediment from subsurface sediment. At the same time, intact maldanids were collected by hand. Sediment was sieved through a 2 mm mesh to remove larger macrofauna and then homogenized. The sediment was then introduced into antfarms by filling with the subsurface sediment until near the intended sediment surface level, and then topping with 2 cm of surface sediment. Sediment was added through water to avoid air bubbles trapped within the sediment. Antfarms were placed in a system with recirculating overlying water, and one or more maldanids were introduced to the sediment surface and allowed to burrow. Individuals that failed to burrow within 24 h were removed from the sediment surface.

"Core aquaria" were 14.6 cm inner diameter polycarbonate tubes, equipped with oxygen sensitive optodes affixed to the inside wall with double-sided adhesive film (X-film DX1). An example of this type of aquarium is shown in Supplementary Fig. 1B. For experiments with intact sediment, these cores were manually pushed approximately 30 cm into the sediment within dense patches of the  $\it C. torquata$  bed, identified by the tube caps protruding from the sediment. The cores were excavated and quickly sealed at the bottom (generally within  $\sim 30~\rm s$  of removal) to prevent porewater drainage, then submerged in water and transported to the lab. Cores were sealed at the bottom with rubber pipe caps and hose clamps and at the top with polycarbonate lids with water exchange ports and integrated magnetic stirring apparatuses that were used to exchange and gently stir the overlying water.

Planar optode imaging was used to assess oxygen dynamics induced by bioirrigation and followed the approaches developed by Polerecky et al. (2005, 2006). O2-sensitive planar optodes were made from platinum porphyrin dye (Pt(II)meso-Tetra(pentafluorophenyl)porphine, Frontier Scientific)—an indicator whose luminescence lifetime under blue light is dependent upon the partial pressure of O2 to which it is exposed—immobilized in a thin polystyrene matrix and attached to the interior of the aquarium (Precht et al., 2004). The luminescence lifetime imaging system (the MOLLI system, originally developed by Holst et al., 1998 and Holst and Grunwald, 2001) was modified by using a different CCD camera (pco.1600MOD, PCO) and a pulse delay generator (T560, Highland Technology), as previously described in Matsui et al. (2011). Blue LEDs ( $\lambda_{max} = 455$  nm, LXHL-LR5C, Philips Lumileds) were used as an excitation light source. Per-pixel oxygen concentrations were calculated using Matlab (version 8.5.0.197613, Mathworks) and images of oxygen and oxygen dynamics were produced and analyzed using Matlab, R (version 3.4.1, The R Project for Statistical Computing), RStudio (version 1.0.153, RStudio), and ImageJ (version 1.50c4, National Institutes of Health; utilities available from authors). Matlab utilities were developed by Polerecky et al. (2005, 2006). R and ImageJ utilities were developed by I. P. Dwyer.

In order to have a second, independent measurement of animal pumping activity, aquaria in one of the experiments were fitted with pressure sensors (Honeywell 26PCAFB6G) (Wethey and Woodin, 2005). Pressure sensors were hydraulically connected to the porewater through water-filled tubing attached to ports in the sidewall of the aquarium, covered internally with a fine mesh to allow water penetration but not sediment infiltration. Interpretation of the pressure records and correlation with  $\rm O_2$  imaging data followed approaches developed by Volkenborn et al. (2010, 2012a, 2012b).

### 2.1.2. Experiments

All experiments were conducted in a temperature-controlled room using different types of aquaria with constructed or intact sediments to assess irrigation activity and oxygen dynamics in different seasons and at different temperatures (summarized in Table 1).

Experiment 1, conducted in July of 2015, assessed burrow morphology, hydraulic activities, and oxygen dynamics in and around *C. torquata* burrows using oxygen imaging and porewater pressure sensors. Individual *Clymenella*, were allowed to establish their burrows in four separate antfarm aquaria with dimensions of approximately 13

Table 1

Pumping patterns by the maldanid polychaete, Clymenella torquata, at different temperatures. Non-bold rows represent the mean and standard deviations of pumping and resting durations of individual worms. Bold rows are the means and standard deviations across maldanids within an experiment/treatment. Duty cycles were calculated as the percentage of time maldanids spent pumping over the average pumping-resting cycles. Pumping and resting durations and standard deviations were rounded to the nearest interval of the resolution at which they were captured (1 or 0.5 min).

Experiment	T (°C)	Pump (min)	SD	Rest (min)	SD	Duty Cycle (%)	SD
Exp 1	15	9	5	6	4	58.1	_
Exp 1	15	6	4	6	6	47.4	_
Exp 1	15	5	4	5	3	53.0	_
Exp 1	15	5	2	5	5	51.0	_
Exp 1	15	6	1	6	1	52.4	3.9
Exp 2 (Field							
Temp)	19	3.5	2.5	3.5	3.5	48.2	_
Exp 2 (Field							
Temp)	19	4.0	2.0	4.5	2.5	47.4	_
Exp 2 (Field							
Temp)	21	3.5	1.0	3.5	1.0	50.3	_
Exp 2 (Field							
Temp)	21	4.5	2.5	3.5	3.0	54.8	_
Exp 2 (Field							
Temp)	20	4	1	4	1	50.1	2.9
Exp 2 (Ramp)	12	7.5	4.5	7.0	3.5	51.7	_
Exp 2 (Ramp)	12	7.0	4.5	5.5	2.5	56.0	_
Exp 2 (Ramp)	12	4.5	2.0	6.0	2.5	43.8	_
Exp 2 (Ramp)	12	6.5	1.5	6.0	0.5	50.5	5.1
Exp 2 (Ramp)	5	14.5	5.0	16.5	6.5	46.7	_
Exp 2 (Ramp)	5	17.5	5.5	15.5	5.5	52.6	_
Exp 2 (Ramp)	5	11.5	4.0	8.5	4.0	57.4	_
Exp 2 (Ramp)	5	14.5	2.5	13.5	3.5	52.3	4.4
Exp 3A							
(Winter)	6	9	5	22	11	29.1	-
Exp 3A							
(Winter)	6	11	5	22	18	32.9	_
Exp 3A							
(Winter)	6	8	4	34	20	18.7	_
Exp 3A							
(Winter)	6	9.0	1.0	26.0	6.0	26.9	6.0
Exp 3B							
(Summer)	21	2.5	1.0	3.5	1.5	43.4	-
Ехр ЗВ							
(Summer)	21	1.5	1.0	1.5	1.0	52.3	_
Exp 3B							
(Summer)	21	2.5	1.5	3.5	2.0	43.4	-
Ехр ЗВ							
(Summer)	21	3.0	1.5	2.5	1.0	56.6	-
Exp 3B							
(Summer)	21	7.0	4.5	6.5	5.5	53.1	-
Ехр ЗВ							
(Summer)	21	3.5	2.0	3.5	1.5	49.7	5.4

cm wide, 24 cm tall, 2.5 cm thick and held at 15  $^{\circ}$ C. Oxygen images of these four antfarms were captured every minute for 14 days with minimal interruption. Each antfarm was also fitted with a porewater pressure sensor to record changes in porewater pressure associated with the maldanids' activities.

Experiment 2, conducted in June of 2019, assessed the role of temperature in spatio-temporal patterns of *Clymenella* bioirrigation using oxygen imaging during an imposed temperature ramp. Seven *Clymenella* individuals were added to an antfarm with dimensions of approximately 32 cm wide, 36 cm tall, 1 cm thick. This antfarm was kept at field temperatures of 19 °C to 22 °C for thirteen days. The temperature was then lowered over the course of a few hours to 12 °C and maintained at this level for three days, and finally lowered to 5 °C, where it remained for four days. Oxygen images of this antfarm were captured every 30 s for 20 days with minimal interruption.

Experiment 3 was split into two parts, A and B, to examine seasonal spatio-temporal patterns of *Clymenella* bioirrigation and the resulting

oxygen dynamics in sediment in winter and summer. In both seasons three intact cores (14.6 cm diameter, 30–40 cm deep) labeled WC1-WC3 and SC1-SC3 for winter and summer, respectively, were collected within dense aggregations of maldanids in the field and kept at field temperatures. Experiment 3A (Winter) was conducted in March of 2020 at 6 °C. In Experiment 3A, 20 additional field-collected animals were added to the core with the lowest apparent density (WC2) at the onset of the experiment. Oxygen images of the cores in Experiment 3A were captured every minute for 11 days with minimal interruption. Experiment 3B (Summer) was conducted in July–August of 2020 at 21 °C. Oxygen images of the cores in Experiment 3B were captured every 30 s for 16 days. At the end of each part of Experiment 3, the sediment in each core was sieved, and animals present were identified and counted.

#### 2.2. Data analysis

Because maldanids create relatively complex burrows, it was important to distinguish different parts of their burrows when analyzing and interpreting O2 data. Maldanid burrows consist of one or sometimes multiple vertical tubes, which typically end in a feeding pocket. These fragile, lined/cemented tubes represent the burrow structures that the animals reside in most of the time and are typically only a few mm in diameter and up to 30 cm long. When present near the aquarium wall, tubes were visible in O2 images as long, usually vertical features with small diameters that showed fairly constant oxygenation when the burrow was ventilated. The feeding pockets at the ends of tubes generally appeared as roughly circular areas where oxygen was detected when worms ventilated their tubes. Because the feeding pockets are not lined, the distribution of O<sub>2</sub> in and around the feeding pocket was more variable than O<sub>2</sub> observed in and around tubes, as pumping of water into the blind burrow end resulted in advective transport of oxygenated water into the surrounding permeable sediment. As maldanids establish a feeding pocket, the porosity locally increases, ultimately leading to feeding voids, which can be refilled by the worm via surface sediment subduction. Supplementary Fig. 2 shows an example of how tubes and feeding pockets are identified and interpreted in oxygen images. A more dynamic view of these structures and how they evolve over time is shown in supplementary video 1. Raw image sets and further information on image processing are available at https://www.bco-dmo. org/dataset/890950 ( 10.26008/1912/bco-dmo.890950.1).

To quantify pumping patterns, oxygen image series from each temperature or treatment within each experiment were selected that showed as many active feeding pockets as possible. All feeding pockets in which irrigation activity was visible for at least 45 min were analyzed. For each visible feeding pocket, a rectangular region of interest (ROI) that enclosed the dynamic region was selected and the average oxygen concentration within the ROI was plotted against time. Times during which the average oxygen concentration within the ROIs was either increasing or remaining constant at a nonzero level were interpreted as active pumping intervals and times during which the average oxygen concentration within the ROIs was either decreasing or remained constant at zero were interpreted as resting intervals (Polerecky et al., 2006). Supplementary Fig. 3 shows an example of such a time-series and how it was interpreted. For each feeding pocket, the durations of at least 7 but typically >20 consecutive pumping and resting intervals were determined (dependent upon what was observable). Based on the mean durations of pumping and resting intervals, the duty cycle for each animal was calculated as the percentage of the time that the animal spent pumping during a mean pumping-resting cycle.

Sedimentary oxygen consumption rates (OCRs) were derived for selected feeding pockets in which oxygen disappeared completely or nearly completely at least once during the selected time series. For each of these pockets, the mean oxygen concentration in a small ROI in the center of the pocket was calculated from when the extent of the oxic pocket was maximal until all oxygen was consumed. OCRs were then estimated based on the linear decline of O<sub>2</sub> over time (Polerecky et al.,

2005). In some experiments, oxic water was manually injected near the aquarium front wall through a long needle connected to a syringe to assess OCRs in sediment regions that had not been supplied with  $O_2$  by maldanid activity during the experiments (Volkenborn et al., 2010, 2012b).

For antfarm experiments with reconstructed sediment, the first week after set-up was excluded from analyses, to allow animals to establish their burrows. This interval was chosen because, based on the oxygen images, the maldanids did not appear to burrow deeper, establish new tubes, or extend existing tubes with great frequency, suggesting they established fully functional burrows. Likewise, the first several days of experiments with intact cores were excluded from analyses to allow recovery from disturbances associated with sampling and transport. Whenever temperature was changed, the initial 24 h of data were excluded from the analyses after the new temperature was established to give animals time to acclimate. For analyses, time-series data were selected during which regular activity patterns were observed to ensure that transitional periods in behavior were not included in the analyses.

To determine spatial utilization by *C. torquata*, oxygen was used as a non-conservative tracer. Because oxygen kinetics, irrigation behavior, and frequency of animal relocation were dynamic, a time-averaged oxygen distribution was not a sensitive enough approach to determine the area affected by maldanids. Therefore, the maximum oxygen concentration for each pixel recorded throughout a time series was determined, resulting in "maximum oxygen" images. The advantage of this approach is that ephemeral oxygenation events and migrating feeding pockets were captured with similar intensity to longer oxygenation events, therefore creating images that display the full spatial extent of sediment oxygenation induced by the animals over a chosen time interval.

For quantitative analysis of spatial utilization, long-term maximum oxygen images were produced using data from intact sediment core incubations. In Experiment 3B, the longest period during which the cores and/or camera were not repositioned was approximately 6 days. A similar period was available Experiment 3A. While these intervals contained short breaks and discontinuities (usually minutes or less, but no more than several hours) that would thwart detailed analysis of oxygen dynamics, it is unlikely that a meaningful amount of activity was missed by a maximum oxygen image, which only stores absolute maxima from the entire image series. Maximum oxygen images were produced covering the same amount of time from both series, corresponding to the maximum time available from Experiment 3B (6 d, 7 h, 13 min). From each core in these images, a 5-cm-wide region of interest close to the center of the optode-camera-facing side of the core was chosen for detailed analysis. After correcting for uneven sediment surface height by aligning the highest surface point of each vertical column of pixels at y = 0, each pixel was determined to be oxic (\ge 10\% air saturation) or anoxic, and a horizontally integrated vertical profile of oxic area (%) was produced. An additional set of "typical" profiles was produced by averaging the three profiles from each season.

For each temperature treatment (antfarms) or season (intact cores) within each experiment, 12 h of uninterrupted sequential data were selected to derive images of per-pixel oxygen dynamics. Images with lighting artifacts, i.e., due to opening/closing of the environmental chamber door were replaced with the nearest frame with no such artifacts. The largest interruption "repaired" this way was 3.5 min long. After generating maximum oxygen images for these 12-h intervals, additional images were generated that display per-pixel oxic probability, redox oscillation frequency, and mean lengths of oxic and anoxic intervals. For event durations, only events with both a start and end observed within the 12-h time period were included in the analysis. In all analyses, "oxic" was defined when the oxygen concentrations was >10% air saturation. This threshold was chosen to exclude image noise, which was not excluded when using a threshold of 5%. As relevant metrics of redox conditions, "oxic probability", "redox oscillation frequency", "mean oxic event duration" were estimated. These metrics were operationally defined and derived from image series as follows

#### (Volkenborn et al., 2012a, 2012b):

*Oxic probability* - Oxic probability was estimated by counting the number of images in the series in which a pixel was oxic and then dividing this number by total number of images.

*Redox oscillation frequency-* Redox oscillation frequency was estimated by dividing the number of observed changes in oxic status (from oxic to anoxic and vice-versa) for each pixel over a given time interval by two and then dividing the result by the length of the time interval and reported as redox cycles per hour.

*Mean oxic event duration* – Mean oxic event duration was estimated by calculating the average duration of oxygen presence at each intermittently-oxic pixel.

To quantitatively analyze the spatio-temporal patterns of sediment oxygenation induced by maldanids, the mean, median, maxima, minima, and the 1st and 99th percentiles of redox oscillation frequencies and mean oxic event durations were determined for each image pixel that experienced intermittent oxygenation during a 12-h period. Pixels that did not experience a complete oxygenation event (start and end) during the measurement interval were excluded from the oxic event duration calculations. These analyses were done separately for different regions of interest (feeding pockets, tubes, sediment-water interface) for each temperature in the temperature ramp experiment (Experiment 2), and for intact winter and summer cores (Experiment 3). The total area included in each analysis was determined by multiplying the number of pixels by the area of a single pixel.

To assess the relationship between redox oscillation frequencies, mean durations of oxic events, and oxic probabilities, amplitude analyses were performed for intact winter and summer cores (Experiment 3) for the same regions of interest. Redox oscillation frequencies were plotted against each of the other two redox metrics on log-log scales (due to the heavily right-skewed nature of the data), and the 2-dimensional kernel densities of pixels were estimated using the R package "MASS" (Venables and Ripley, 2002) and plotted using the package "ggplot2" (Wickham, 2016). "Naïve" predictions of oscillation frequency in cycles per hour (60 / [mean pumping duration in minutes + mean resting duration in minutes]), oxic event duration (mean pumping duration in minutes), and oxic probability (duty cycle expressed as a %) were made for winter and summer pockets and tubes using the pumping and resting patterns measured for each season in Experiment 3 and plotted along with the data points and kernel density for comparison. The same predictions were made and plotted for surface sediments but switching the roles of pumping and resting in the calculations, as irrigation at depth in the sediment results in the shallowing of the oxygen penetration depth near the sediment-water interface.

# 2.3. Statistical analyses

Statistica (version 13.5.0, TIBCO Software, Inc.) was used to perform one-way ANOVA analyses to test the effects of temperature (Experiment 2) or season (Experiment 3) on pumping durations, resting durations, and OCRs. The same procedure was used to test for effects of treatment across all experiments on duty cycles. If data were non-normally distributed or had inhomogeneous variances between the tested groups, Box-Cox transformations were used to fulfill ANOVA assumptions. If applicable, Tukey's HSD tests were used to determine which groups differed significantly (or unequal N HSD tests where appropriate).

# 3. Results

# 3.1. Population densities of Clymenella in experiments

In Experiment 1, single maldanids were present in each antfarm, corresponding to a population density of 308 individuals/m<sup>2</sup>. In Experiment 2, all seven of the individuals initially added to the antfarm were recovered at the experiment end, corresponding to a population

density of 2188 individuals/m². In Experiment 3A, cores WC1, WC2, and WC3 contained 43, 49, and 37 *Clymenella* individuals, respectively, corresponding to densities of 2570, 2930, and 2210 individuals/m² at the experiment's conclusion (initial population unknown). Most recovered animals were of roughly the same relatively large size ( $\geq 5$  cm length), functionally defined as "adults". In Experiment 3B, cores SC1, SC2, and SC3 contained 20, 23, and 44 *Clymenella* individuals, respectively, corresponding to densities of 1195, 1374, and 2628 individuals/m² at the experiment's conclusion (initial population unknown). Unlike in Experiment 3A, the animals recovered from the cores in Experiment 3B were of two distinct size classes, functionally defined as "adult" ( $\geq 5$  cm length) and "juvenile" (<5 cm length), with juveniles making up 45%, 70%, and 75% of the individuals in cores SC1, SC2, and SC3, respectively.

# 3.2. Oxygen dynamics and porewater pressure dynamics induced by individual maldanids

In Experiment 1,  $O_2$  imaging started 3 days after individual  $C.\ torquata$  were added to 4 antfarm aquaria. By this time, all individuals had established a feeding pocket centered between 15 and 17 cm depth that were visible as circular, intermittently oxygenated regions with area up to  $10\ cm^2$  (Fig. 1A). Oxygen concentrations in the center of these pockets reached  $O_2$  concentrations of up to 60% air saturation, and oxygen concentrations varied in parallel with the wax and wane of the oxic spheres (Fig. 1B). In addition to the oxygen dynamics at depths, the location of the oxic-anoxic boundary at the sediment water interface changed dynamically, including events during which oxic water was drawn down across most of the sediment surface. In some cases, this drawdown was accompanied by anoxic water being detected above the sediment surface, apparently expelled from maldanid tubes (Fig. 1A).

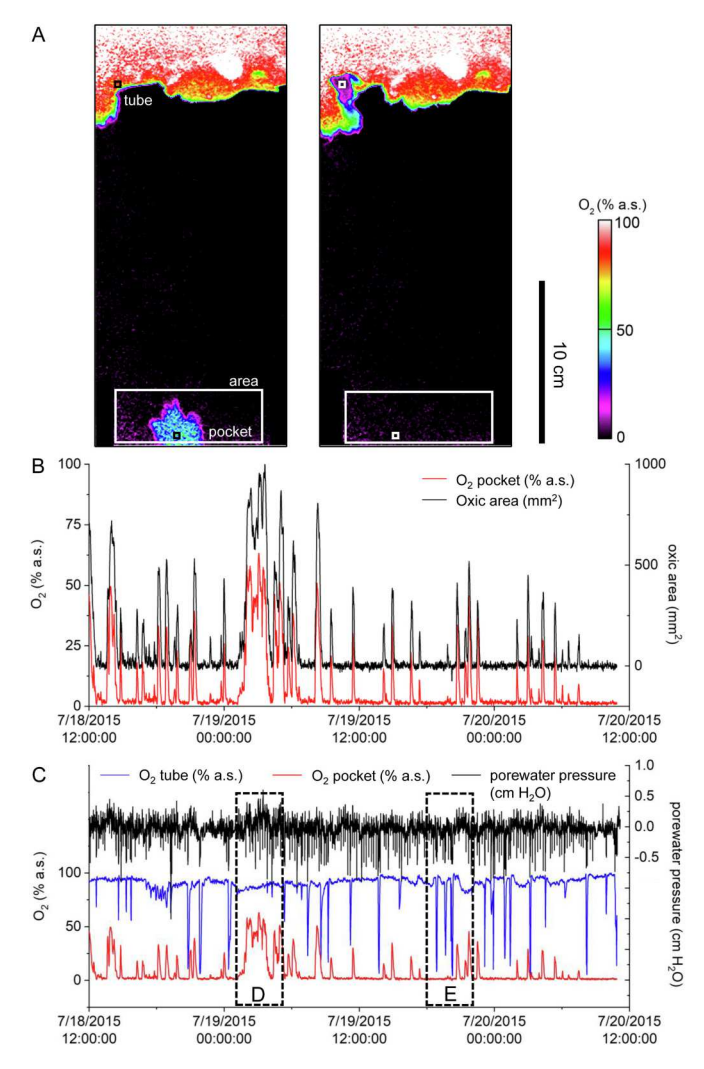
Oxygen dynamics were closely related to porewater pressure dynamics (Fig. 1) and a 2-day porewater pressure record was analyzed in more detail. During 87% of the time, porewater pressure was affected by the maldanid with only short periods of complete inactivity (average duration of inactivity was  $2.7 \pm 1.4$  min with a frequency of  $2.8 \ h^{-1}$ ). The porewater pressure record was characterized by short negative pressure pulses, followed by positive porewater pressurization. These short-term negative pressure pulses typically lasted  $2.3 \pm 0.7$  s (n=10) and occurred on average every 13.6 min (i.e.,  $4.4 \ h^{-1}$ ). Periods of positive pressurization with short negative pulses were accompanied by intense oxygenation of the feeding pocket (Fig. 1D). Time periods when anoxic water was pushed out the tube were accompanied by longer periods of negative porewater pressure (Fig. 1E), lasting on average for  $3.0 \pm 1.4$  min. 17.7 of these negative porewater pressure events were recorded per day (i.e., 0.7/h).

# 3.3. Pumping patterns based on $O_2$ data

Seasonal differences in pumping patterns were detected in Experiment 3. The durations of pumping and resting differed significantly between the intact, in-season cores in Experiment 3A (Winter) and Experiment 3B (Summer) (pumping:  $F_{1,6} = 14.3$ ; p < 0.01; resting  $F_{1,6} = 61.5$ ; p < 0.001). The average observed pumping/resting patterns were 9 min/26 min in winter at 6 °C and 3.5 min/3.5 min in summer at 21 °C (Table 1, Fig. 2A–B).

Likewise, temperature was a significant factor explaining pumping and resting durations during the temperature ramp in Experiment 2 (pumping:  $F_{2,7}=38.3;\,p<0.001;$  resting:  $F_{2,7}=45.4;\,p<0.001).$  The average duration of pumping/resting were 4 min/4 min, 6 min/6 min, and 15 min/14 min at 19–21 °C, 12 °C, and 5 °C, respectively (Table 1, Fig. 2A–B), and both pumping and resting durations were significantly different between all three temperature treatments (Tukey post-hoc p<0.05).

The summer-collected sediment and animals used in Experiment 2 showed similar pumping and resting durations at  $19-21~^\circ C$  to those



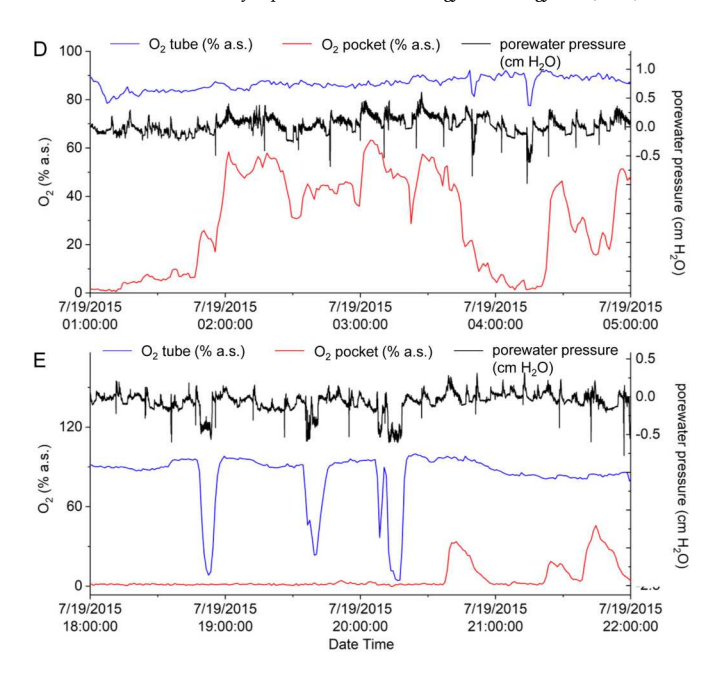


**Fig. 1.** Porewater pressure and related oxygen dynamics in sediments with an individual *Clymenella torquata*. Panel A shows oxygen images from an antfarm during a forward pumping (left) and backward pumping event (right). Panel B shows the size of the oxic area around the feeding pocket within the large rectangles and the oxygen concentrations measured in the small squares in the center of the feeding pocket over the 2-day period. Panel C shows the oxygen concentrations measured within the intermittently oxic pocket and close to the tube opening above the sediment surface together with the porewater pressure record. To highlight the relationship between porewater pressure and oxygen dynamics two selected 4-h periods are shown in panels D and E emphasizing the link between increasing oxygen concentrations in the feeding pocket during positive porewater pressurization and the discharge of anoxic water through the maldanid tube during negative porewater pressurization.

observed in the summer-collected intact cores used in Experiment 3B at 21 °C (pumping:  $F_{1,7}=0.97;\ p=0.36;$  resting:  $F_{1,7}=0.39;\ p=0.55).$  However, when summer-collected sediments were cooled to 5 °C, pumping durations were significantly different from those observed in the intact winter-collected cores used in Experiment 3A at 6 °C ( $F_{1,4}=10.1;\ p=0.03)$ , and resting durations displayed a marginally significant difference ( $F_{1,4}=6.94;\ p=0.06$ ) (Table 1, Fig. 2A–B).

Duty cycles differed significantly with treatment across all experiments ( $F_{5,16}=8.64$ ; p<0.001), and this significant difference was largely due to duty cycles in Experiment 3A (winter) with a mean of 27%. This duty cycle was much lower than in all other groups (Tukey post-hoc p<0.003), in which summer-collected sediment and animals were used and duty cycles were all similar to one-another at 50–52% (Tukey post-hoc p>0.97) (Table 1, Fig. 2C).

# 3.4. Spatial utilization

Based on the 12-h maximum  $O_2$  images, it is apparent that feeding pockets in summer (Experiment 3B) were established mostly at relatively shallow depths in the sediment, and sediment oxygenation had a

relatively small spatial extent with typical pocket diameters of ~5–10 mm when compared to pockets in winter (Experiment 3A), which were present deeper in the sediment typically showed a greater spatial extent of oxygenation (20-30 mm diameter) (Supplementary Fig. 6, Supplementary Data: SeasonalComparison.mp4). As temperature was ramped down in Experiment 2, maldanids rapidly (within 8 h of the being set from 21 °C to 12 °C) deepened their feeding pockets, and the size of oxygenated pockets increased (Supplementary Fig. 7A-C). Consequently, spatial utilization patterns in Experiment 2 resembled those observed in summer at 21 °C (Experiment 3B) (Supplementary Figs. 6A, 7A) and transitioned to resembling oxygenation patterns in winter at 12 °C and 5 °C (Experiment 3A) (Supplementary Figs. 6B, 7B-C). Experiment 1, which consisted of summer-collected sediments that were cooled to below field temperatures, also showed winter-like spatial utilization patterns at 15 °C, with most individuals establishing feeding pockets close to the bottom of the aquaria, approximately 20 cm below the sediment surface (Supplementary Figs. 6B, 7D).

To get a more comprehensive picture of the spatial extent of sediment oxygenation in summer and winter within a dense maldanid bed, maximum  $O_2$  images were calculated for a 6.3-day period during both

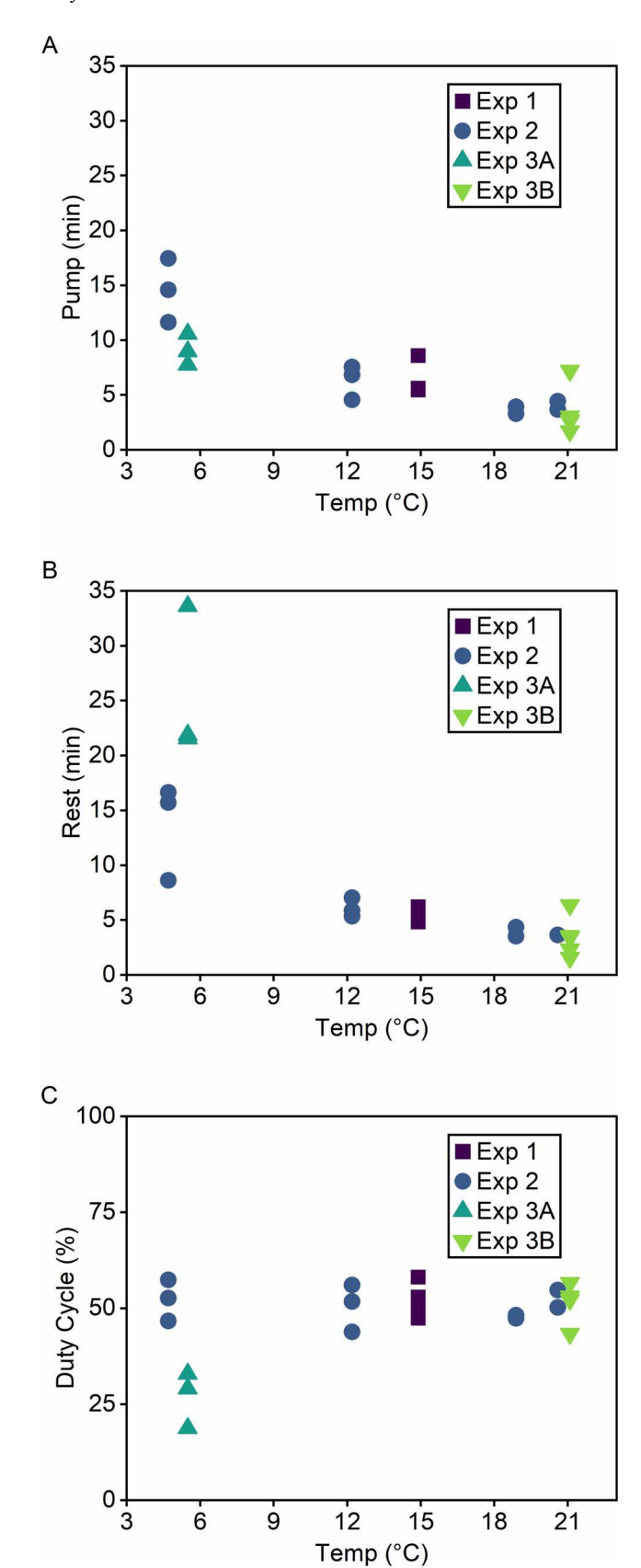


**Fig. 2.** Pumping and resting patterns measured in Experiments 1–3. Mean pumping interval lengths (A), mean resting interval lengths (B), and calculated duty cycles (C) of individual maldanids across all experiments are displayed as a function of temperature.

intact core incubations, thus including relocations of feeding pockets. In summer, maximal  $\rm O_2$  concentrations were typically <50% air saturation and mostly constrained to shallower depth, while in winter comparably large areas reached  $\rm O_2$  concentrations of 50–70% air saturation deeper within the sediment (Fig. 3, Supplementary Data: SeasonalComparison. mp4).

Vertical profiles of oxygen exposure probabilities (i.e., % pixels along a 5 cm horizontal row of pixels exposed to O<sub>2</sub> over the 6.2-day period) varied between individual cores in both seasons (Fig. 4A), but the averaged profiles indicate that sediment oxygenation was largely constrained to the top 10 cm in summer, while a clear subsurface peak was found between 10 and 20 cm in winter (Fig. 4B). Assuming that these average profiles of 2-dimensional data are representative of 3-dimensional conditions, this would mean that during summer, ~25-100% of the sediment at any given depth in the upper 8 cm experiences at least one oxygenation event over a 6.2-day period and that the likelihood of such oxygenation events gradually decreases with depth. In winter, by contrast, oxygenation in the upper 10 cm of the sediment was less prevalent, but there was a  $\sim 10$ –40% chance of sediment oxygenation at depths between 10 and 20 cm over the 6.2-day period. The 10% threshold chosen to define oxic conditions in this study likely resulted in a slight underestimation of the areas supplied with oxygenated water, as the true oxic-anoxic boundary would exist further into the sediment surrounding the irrigated pockets. However, this artifact should be small, given the steep O2 gradients, and it seems plausible that the redox metrics determined by this approach are a reasonable approximation of the spatial extent of redox dynamics in the studied sediments.

#### 3.5. Spatio-temporal oxygen dynamics

#### 3.5.1. Oxygen consumption rates (OCR)

Overall, OCRs varied substantially between pockets at the same temperature, but OCRs were significantly affected by temperature during the temperature ramp in Experiment 2 ( $F_{2,6}=16.9;\,p<0.01$ ) with significantly higher OCRs at 21 °C (mean  $\sim12.8~\mu\text{M/min}$ ) than at 12 °C (mean  $\sim1.9~\mu\text{M/min}$ ) and 5 °C (mean  $\sim1.3~\mu\text{M/min}$ ) (Table 2). In contrast, OCRs measured in pockets in intact sediments (Experiment 3) did not differ significantly between summer at 21 °C (mean  $\sim5.8~\mu\text{M/min}$ ) and winter at 6 °C (mean  $\sim3.0~\mu\text{M/min}$ ) ( $F_{1,4}=0.28;\,p=0.63$ ).

OCRs measured after artificial water injection into bulk sediment in Experiment 2 at 5 °C were significantly higher (mean  $\sim6.3~\mu\text{M/min})$  than OCRs measured around maldanid feeding pockets (mean  $\sim1.3~\mu\text{M/min})$  (F1,3 =93.1;~p<0.01)). Likewise, OCRs were 2-fold higher after artificial water injection into bulk sediment (mean  $\sim14.4~\mu\text{M/min})$  than around feeding pockets (mean  $\sim5.8~\mu\text{M/min})$  in Experiment 3B at 21 °C, but due to limited replication and high variability this difference was not significant (F1,4 =4.25;~p=0.11).

#### 3.5.2. Redox dynamics

In intact summer cores and in the 21 °C phase of the temperature ramp, feeding pockets generally experienced redox oscillations throughout their volumes, while feeding pockets in winter cores and at  $12^{\circ}$  and 5 °C in antfarms tended to oscillate primarily at their outer edges in shells  $\sim 1-8$  mm thick while remaining continuously or near-continuously oxic throughout most of their volumes (Fig. 5, Supplementary Fig. 4. Supplementary Data: SeasonalComparison.mp4). Similarly, sediment adjacent to tubes tended to remain oxic, oscillating only at their edges in zones  $\sim 1-2$  mm thick (Fig. 5, Supplementary Fig. 4, Supplementary Data: SeasonalComparison.mp4). Feeding pockets in Experiment 1 at  $15^{\circ}$ C experienced oscillation throughout their volumes, but some displayed elevated frequencies at their edges (Supplementary Fig. 5).

All measured distributions of redox oscillation frequencies and oxic event durations were heavily right-skewed, meaning that they were strongly biased toward the lower end of their ranges, but there were notable differences between them. In Experiment 3, redox oscillation

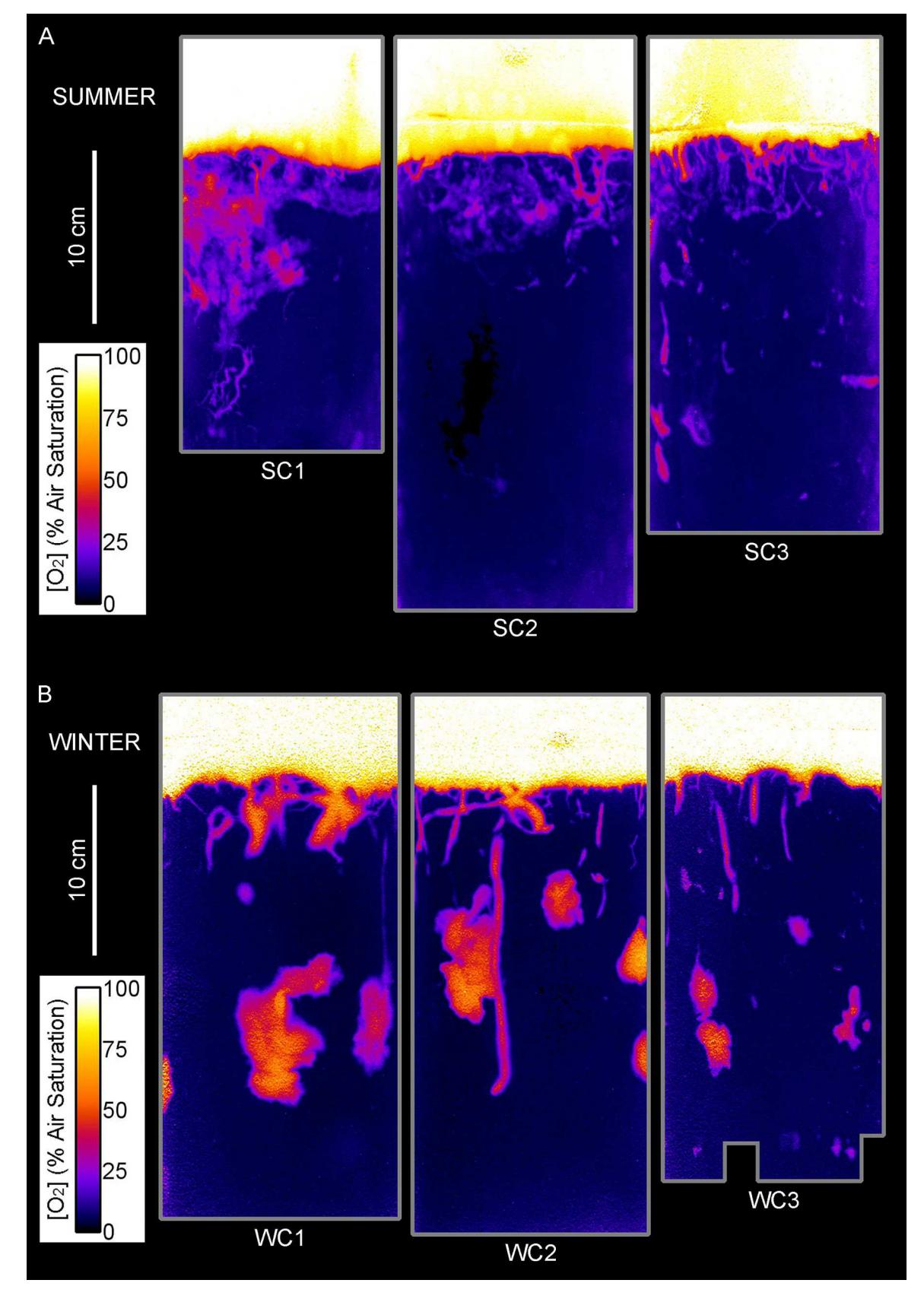
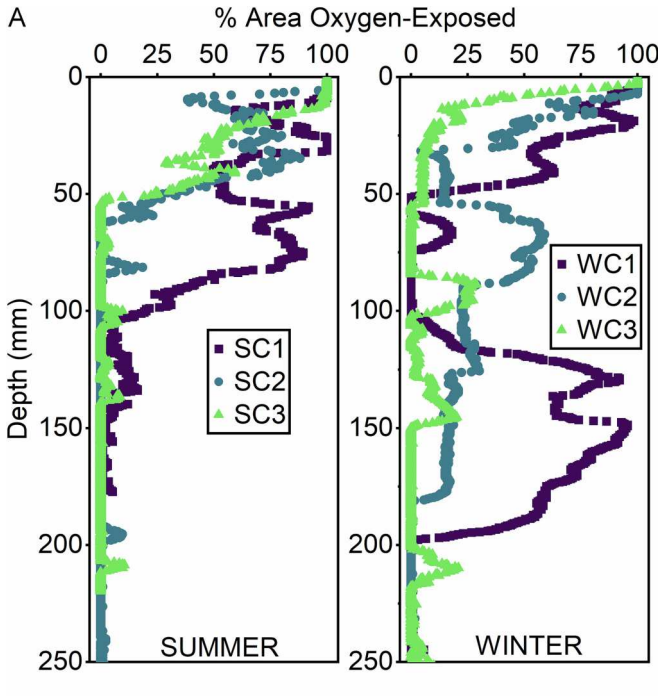
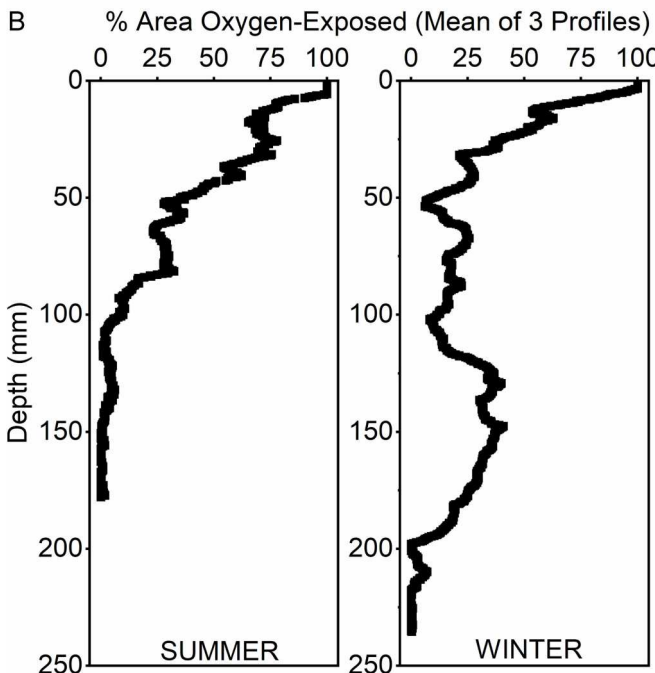


Fig. 3. Spatial extent of intermittent sediment oxygenation as derived from maximum  $O_2$  measurements in three parallel intact sediment cores with *Clymenella torquata* over  $\sim$ 6.3 days in summer (A) and winter (B). High-frequency, high-amplitude imaging noise accumulated by the maximum  $O_2$  measurement procedure causes some completely anoxic areas of cores to appear to have experienced oxygenation up to  $\sim$ 10% air saturation. Consequently, values this low and lower should be considered functionally anoxic for the purposes of interpreting this figure.





**Fig. 4.** Individual (A) and averaged (B) vertical profiles of sediment oxygenation in intact sediment cores with multiple *Clymenella torquata* measured over 6.3 days in summer (left column) and winter (right column). The vertical profiles give the % of pixels that were exposed to oxic conditions in each horizontal line of pixels over a 5 cm wide area. Core labels in panel A correspond to the cores depicted in Fig. 3. The profiles in panel B are each the means of the three corresponding profiles from panel A over the vertical range where all three constituent profiles contained data.

frequencies in feeding pockets and around tubes were much lower in winter (median 0.7/h and median 1.1/h, respectively) than in summer (median 1.2/h and median 2.1/h, respectively), and the distributions (1–99%) of frequencies in summer were more than six times as wide as winter in pockets and more than twice as wide as winter around tubes (Fig. 6A). However, the area affected by the lower frequency oscillations in winter was almost 3 times larger than the area affected by the more

Table 2
Sedimentary oxygen consumption rates as a function of temperature. Oxygen consumption rates were estimated from the linear slope of the oxygen concentration decline within a pocket after irrigation stopped or within an area after water was injected with a needle close to the planar oxygen optode.

Experiment	Source	Temp (°C)	Salinity	OCR (µM/min)
Exp 1	Oxic pocket	15	25	2.9
Exp 1	Oxic pocket	15	25	3.6
Exp 1	Oxic pocket	15	25	3.0
Exp 2 (Field Temp)	Oxic pocket	21	25	14.5
Exp 2 (Field Temp)	Oxic pocket	21	25	16.6
Exp 2 (Field Temp)	Oxic pocket	21	25	7.1
Exp 2 (Ramp)	Oxic pocket	12	25	1.3
Exp 2 (Ramp)	Oxic pocket	12	25	1.5
Exp 2 (Ramp)	Oxic pocket	12	25	3.0
Exp 2 (Ramp)	Oxic pocket	5	25	2.5
Exp 2 (Ramp)	Oxic pocket	5	25	0.5
Exp 2 (Ramp)	Oxic pocket	5	25	0.8
Exp 2 (Ramp)	Injected water	5	25	6.1
Exp 2 (Ramp)	Injected water	5	25	6.6
Exp 3A (Winter)	Oxic pocket	6	30	5.6
Exp 3A (Winter)	Oxic pocket	6	30	1.4
Exp 3A (Winter)	Oxic pocket	6	30	1.9
Exp 3B (Summer)	Oxic pocket	21	30	3.3
Exp 3B (Summer)	Oxic pocket	21	30	12.6
Exp 3B (Summer)	Oxic pocket	21	30	1.5
Exp 3B (Summer)	Injected water	21	30	19.1
Exp 3B (Summer)	Injected water	21	30	12.5
Exp 3B (Summer)	Injected water	21	30	11.5

frequent oscillations in summer (Fig. 6A). Oxic event durations associated with pockets and tubes were longer in winter (median 11.3 min and median 5.3 min, respectively) than those in summer (median 1.1 min and median 1.3 min, respectively) (Fig. 6B). Surface sediments in Experiment 3 showed a similar seasonal pattern to tubes and pockets with regard to redox oscillation frequencies (lower median and less than half as widely distributed in winter) but showed a less clear agreement with patterns of oxic event durations in pockets and tubes (higher median but less widely distributed in winter) (Fig. 6A–B). While it was season-dependent whether pockets or tubes displayed longer event durations or higher oscillation frequencies compared to one-another, surface sediments in each season always displayed both the highest median redox oscillation frequency and the longest median oxic event duration (Fig. 6A–B).

During the temperature ramp (Experiment 2), sediments did not show a clear or consistent pattern with temperature in terms of both redox oscillation frequencies and pumping event durations (Fig. 6C–D). In almost all cases, these redox oscillation frequencies were more similar to Experiment 3B (summer) frequencies than Experiment 3A (winter) frequencies (Fig. 6C). Oxic event durations in antfarms did not consistently resemble summer or winter durations from Experiment 3, but at times were similar to both, with the longest durations occurring at  $12\,^{\circ}\text{C}$  and shorter durations at  $21\,^{\circ}\text{C}$  and  $5\,^{\circ}\text{C}$  (Fig. 6D).

Based on observed pumping patterns in Experiment 3A, typical intermittently-oxic winter sediments were predicted to have an oscillation frequency of ~2 cycles/h, oxic event duration of ~9 min (pockets & tubes) or ~26 min (surface), and oxic probability of ~27% (pockets & tubes) or ~73% (surface). Similarly, based on pumping patterns in Experiment 3B, typical intermittently-oxic summer sediments were predicted to have an oscillation frequency of ~9 cycles/h, oxic event duration of ~3.5 min (pockets, tubes, & surface), and oxic probability of ~50% (pockets, tubes, & surface). Amplitude analyses, performed to visualize the distributions and relationships of these dynamics in surface, tube, and pocket sediments in each season, revealed that these predictions generally hold true. With regard to the most typical combinations of redox oscillation rates and oxic event durations, naïve predictions were very close to accurate in all cases (Fig. 7) except for winter surface sediments (Fig. 7B) (where oscillation rate was underestimated and oxic event duration was overestimated) and summer

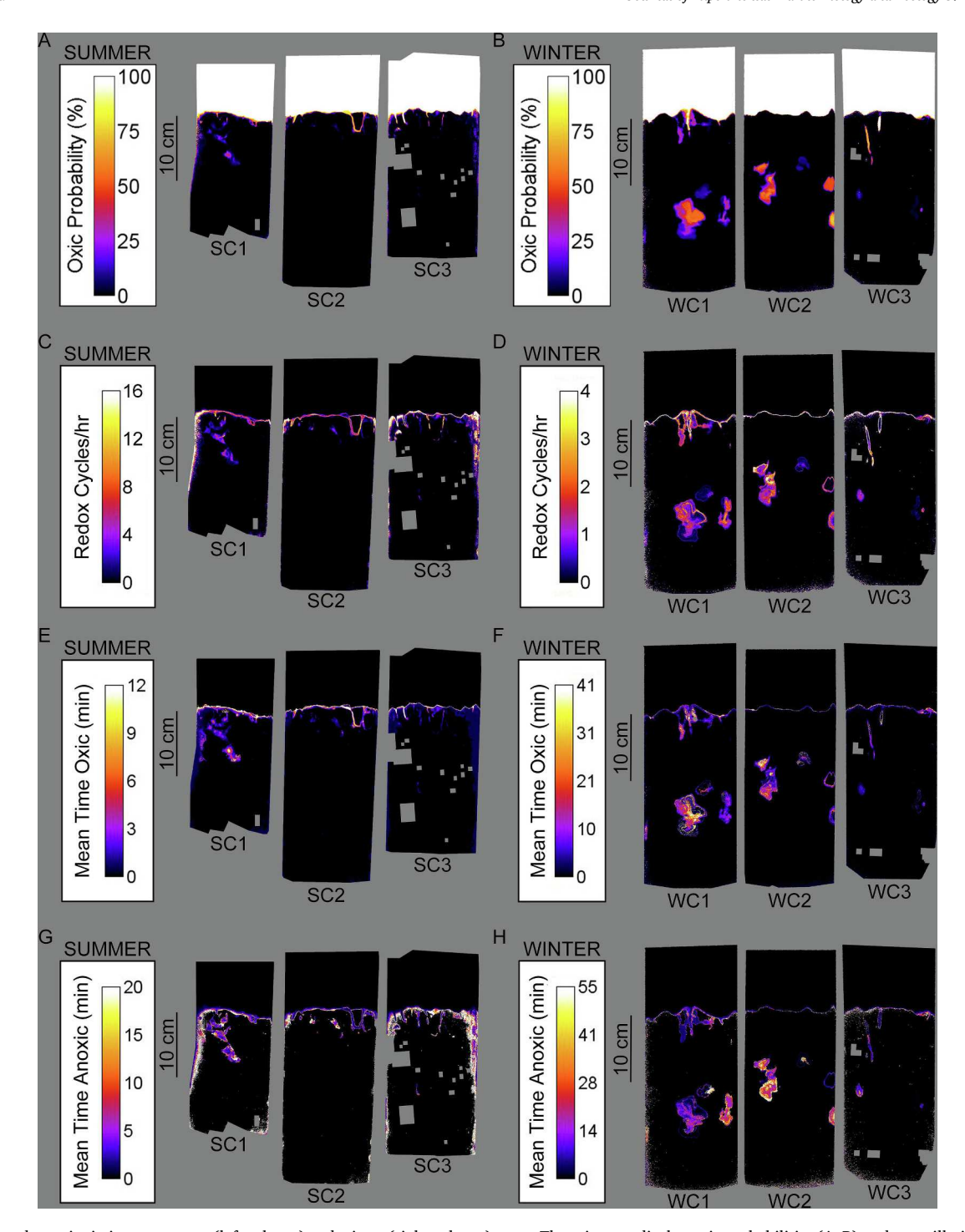


Fig. 5. Oxygen dynamics in intact summer (left column) and winter (right column) cores. These images display oxic probabilities (A, B), redox oscillation frequencies (C, D), mean duration of oxic intervals (E, F), and mean duration of anoxic intervals (G, H) measured at each pixel during an uninterrupted 12-h period (the same period used to construct Fig. 2). For oxic and anoxic interval durations, only events captured in their entirety during the 12-h period were considered. Gray areas mask regions with imaging artifacts which were excluded from the analyses. Some imaging artifacts remain near the edges of some images, especially in summer images, due to the curvature of cores and the angle at which the images were captured.

pocket sediments (Fig. 7E) (where both parameters were severely overestimated). Irrigation-pattern-based predictions were also reasonably good for combinations of redox oscillation frequencies and oxic probabilities in most cases (Fig. 8), once again with the exception of summer pocket sediments (Fig. 8E) (where both parameters were overestimated).

# 4. Discussion

4.1. The use of oxygen as a non-conservative tracer of bioirrigation activity

Oxygen as a non-conservative tracer provides valuable data on bioirrigation activity. Experiment 1 demonstrated a clear direct correspondence between irrigation behavior measured with porewater

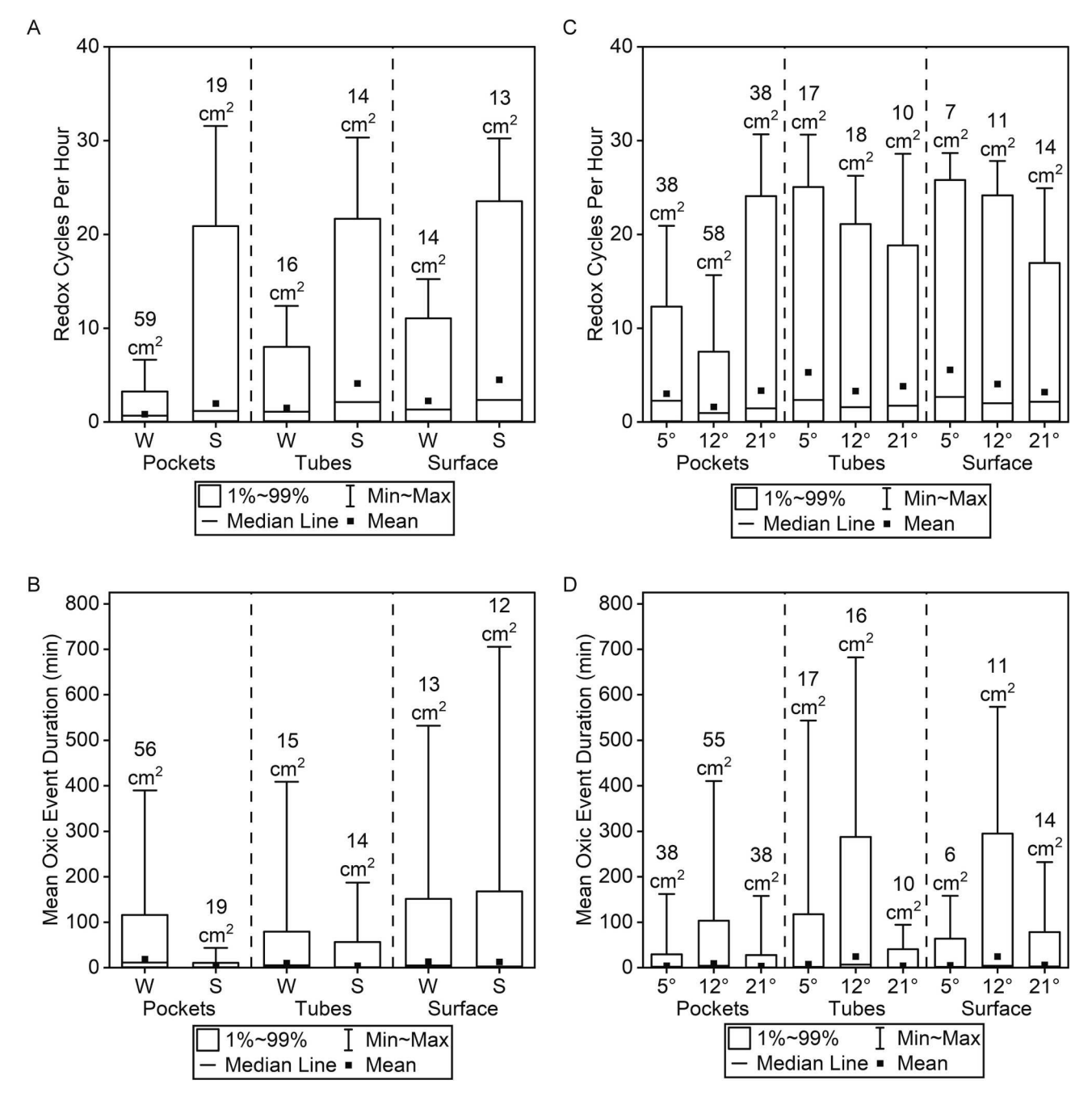


Fig. 6. Redox oscillation frequencies (A, C) and oxic event durations (B, D) in sediments experiencing intermittent oxygenation in intact cores in summer and winter (A, B) and in an antfarm at three different temperatures (C, D). Box and whisker plots display the distribution of redox cycle frequencies (cycles/h) and oxic event durations in pockets and tubes as well as at the sediment-water interface (surface). Each box is labeled at the top of its upper tail with the area of sediment at the optode that is represented by the distribution. Oxic-anoxic oscillation frequencies shown represent the per-pixel mean number of oxic-anoxic cycles experienced per hour (cycles/h) over the 12-h observation. Only those pixels that experienced a nonzero oscillation frequency were considered in this analysis. Oxic event durations shown represent the per-pixel mean duration of oxic events (minutes). Only those pixels for which a full oxic event (start through end) was observed during the 12-h observation were considered in this analysis. In practice, this means that the areas represented by redox frequency distributions are sometimes slightly larger than the areas represented by the corresponding oxic event duration distributions.

pressure sensors and oxygen concentration dynamics measured by oxygen imaging (Fig. 1). This is consistent with previous studies in which both methods were combined (Volkenborn et al., 2010, 2012a, 2012b) and resembles results from Forster and Graf (1995), which indicated a strong correlation between thermistor probes and microsensor oxygen concentration measurements associated with intermittent pumping by bioirrigators. Oxygen imaging alone does not allow confident distinction between backward pumping and a lack of pumping, but forward pumping was clearly distinguishable as increasing or constant nonzero

oxygen concentration in a region of interest located at the center of a feeding pocket (Fig. 1). With regard to the accuracy of the technique in quantifying pumping behavior, aside from the direct correspondence observed in Experiment 1 (Fig. 1), the 12  $^{\circ}\text{C}$  portion of the temperature ramp in Experiment 2 showed pumping cycle periods of 11–15 min, which overlaps with the low end of the range of 15–33 min reported by Mangum (1964) at 12.5  $^{\circ}\text{C}$ , indicating that these results are consistent across methods and realistic.

The primary merits of imaging as a method for quantifying

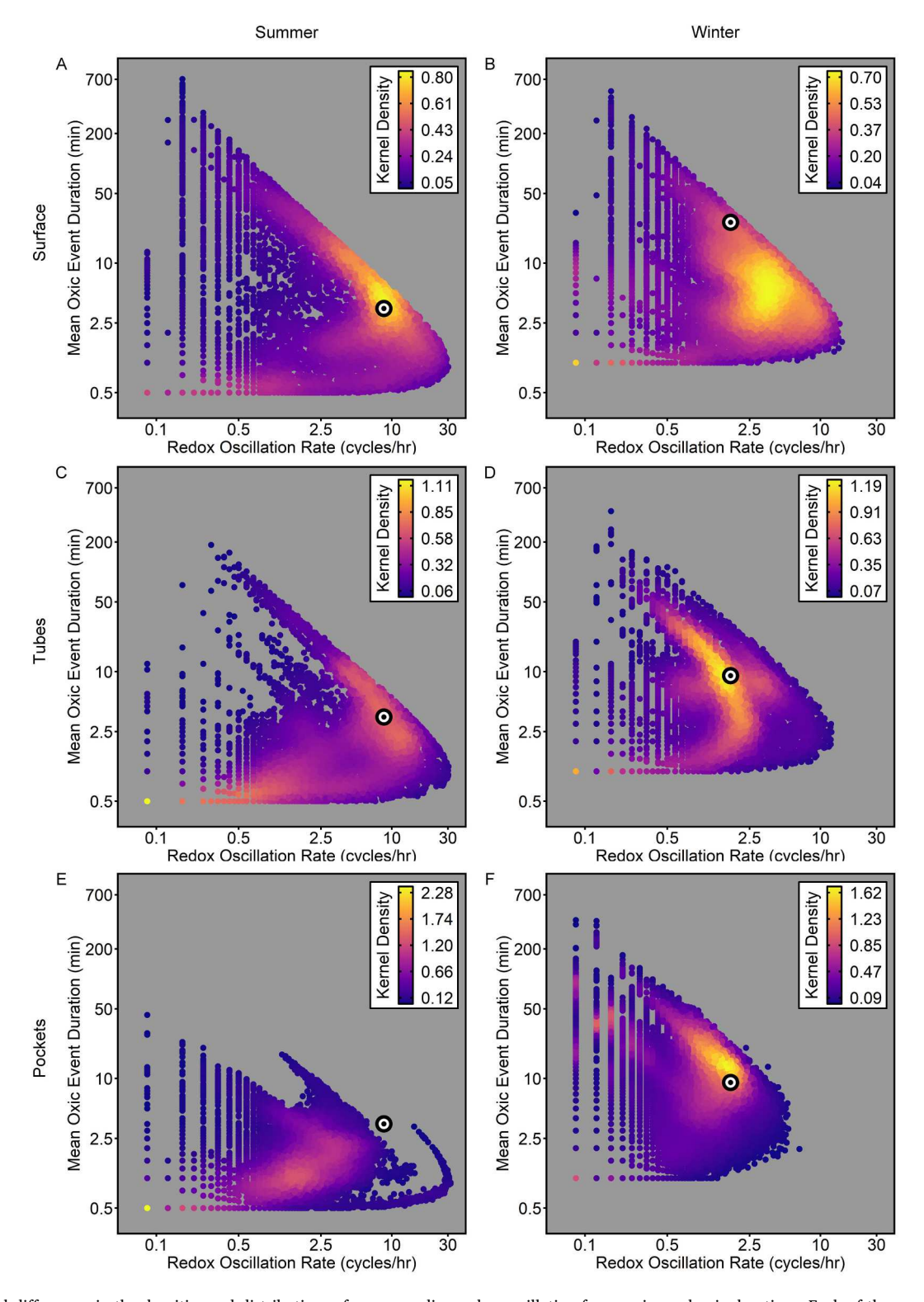


Fig. 7. Seasonal differences in the densities and distributions of corresponding redox oscillation frequencies and oxic durations. Each of the panels in this figure displays a plot of all intermittently-oxic pixels observed in a region of interest over a 12-h period in Experiment 3 based on their redox frequencies (cycles/h) and mean oxic event durations (minutes). Data are presented on log scales due to their highly right-skewed distributions (numbers on axes are not log-transformed). The color of each point represents the calculated kernel density of points at its coordinates within the plot. Panels in the left column represent summer conditions (Experiment 3B) at the sediment surface (A), in/around tubes (C), and in feeding pockets (E). Panels in the right column represent winter conditions (Experiment 3A) at the sediment surface (B), in/around tubes (D), and in feeding pockets (F). In each plot, the predicted location of most typical oxygen dynamics based on naïve predictions from mean pumping and resting patterns are indicated by black-and-white bullseyes.

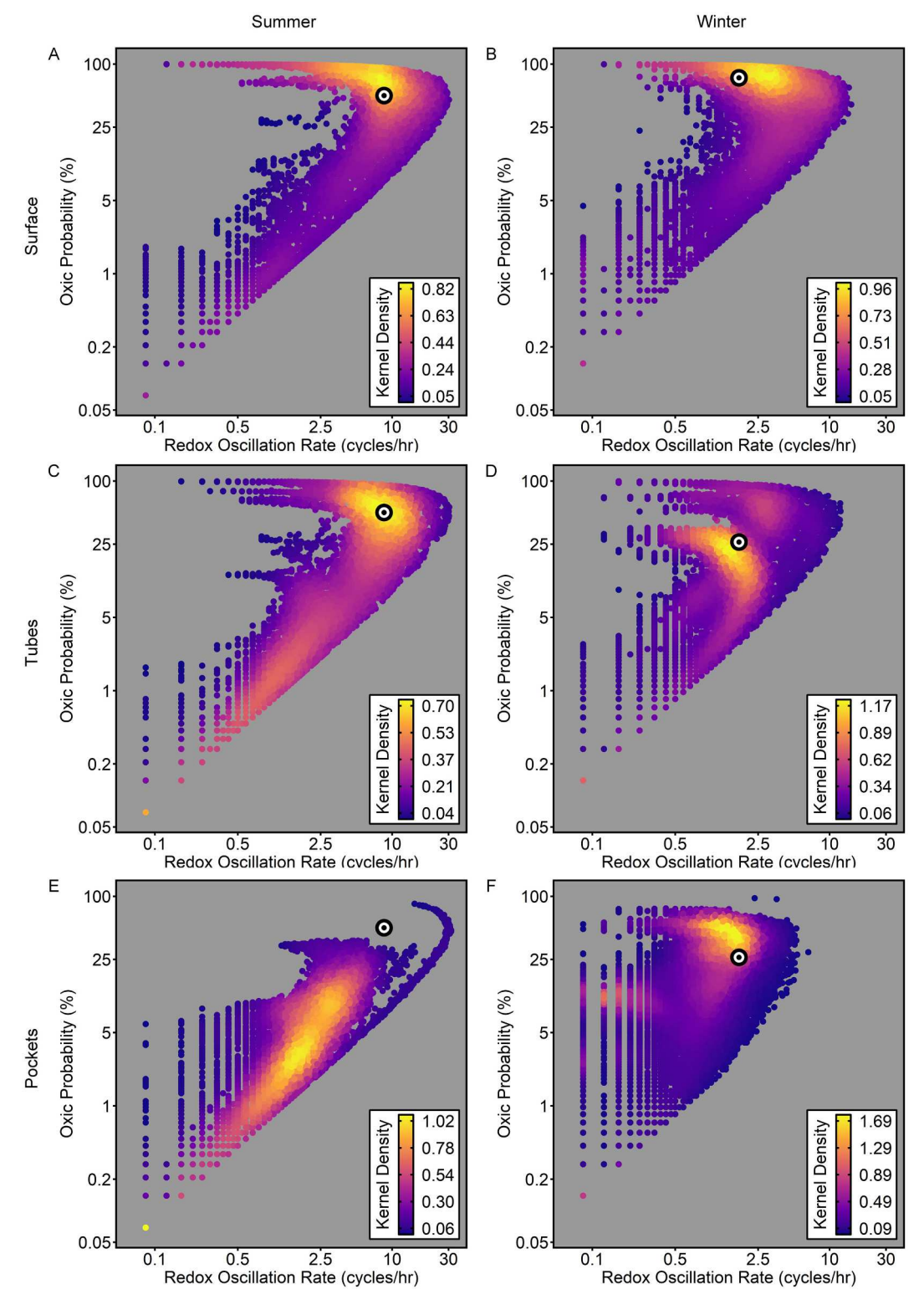


Fig. 8. Seasonal differences in the densities and distributions of corresponding redox oscillation frequencies (cycles/h) and oxic probabilities (%). Each of the panels in this figure displays a plot of all intermittently-oxic pixels observed in a region of interest over a 12-h period in Experiment 3 based on their redox frequencies and oxic probabilities. Data are presented on log scales due to their highly right-skewed distributions (numbers on axes are not log-transformed). The color of each point represents the calculated kernel density of points at its coordinates within the plot. Panels in the left column represent summer conditions (Experiment 3B) at the sediment surface (A), in/around tubes (C), and in feeding pockets (E). Panels in the right column represent winter conditions (Experiment 3A) at the sediment surface (B), in/around tubes (D), and in feeding pockets (F). In each plot, the predicted location of most typical oxygen dynamics based on naïve predictions from the mean pumping and resting patterns are indicated by black.

bioirrigation behavior are twofold: First, multiple animals or an entire intact community may be kept in the same aquarium and imaged simultaneously, and each individual's behavior can be distinguished from the others' by measuring oxygen concentrations in each feeding pocket. Second, imaging provides information on the spatial extent and distribution of oxygen dynamics induced by the observed irrigation patterns, even allowing for the singling-out and independent analysis of specific burrow regions and features. An important caveat, however, is that patterns of oxygenation measured via this method have an inherent detection limit due to imaging noise. In the case of this study, the signal: noise ratio necessitated the functional definition of "oxic" at 10% air saturation, as a lower threshold would have included significant amounts of noise in the final result. Consequently, this method is less reliable for determining dynamics when oxygen concentrations fall in a relatively low and narrow range.

While temperature affected sedimentary oxygen consumption rates in some cases, like in pockets in Experiment 2, the pronounced pocketto-pocket OCR variability within the same treatment as well as between bulk and animal-affected sediments (Table 2, Fig. 2) indicates pronounced biogeochemical heterogeneity, even within initially homogenized sediment. The inability to distinguish between backward pumping and lack of pumping from images may in part explain the pronounced variability of OCRs estimated in feeding pockets, though efforts were made to avoid such artifacts as backward pumping is typically associated with a rapid contraction of oxic spheres rather than an even oxygen concentration decline. The heterogeneity of oxygen consumption rates at similar locations in the sediment likely reflects natural heterogeneity of sediment characteristics (e.g., organic carbon quality and abundance, microbial abundance and community composition—both of which were likely affected by previous flushing and exposure to oxygen). The fact that pocket and bulk sediments can have such different OCRs in initially homogenized, constructed sediment suggests that modifications by animals play a role in creating this heterogeneity. More specifically, the oxygen exposure history of sediment likely correlates with organic carbon depletion through enhanced aerobic respiration and through efficient removal of dissolved reduced species resulting from irrigationinduced advection (Banta et al., 1999; van de Velde and Meysman, 2016). In addition, the OCR measurements are based on oxygen concentration declines in the porewater. Maldanids locally increase porosity within feeding pockets through removal of particles during feeding (Sanders et al., 1962), therefore allowing for the presence of more oxygenated water in a given sediment volume while simultaneously having less grain surface area to which microbes can be attached and contribute to OCRs. These findings highlight that maldanids—and likely many other infaunal organisms—create zones around their burrows that constitute a less oxygen-demanding microhabitat, which may lower the irrigation effort necessary to support their respiratory needs.

# 4.2. The role of temperature in controlling burrow irrigation patterns and depths

From the data presented here, it is evident that both spatial and temporal bioirrigation patterns by *C. torquata* are subject to seasonal variation. Temperature plays an important role for the spatio-temporal patterns of sediment oxygenation, as the lengths of pumping and resting intervals and the depths of irrigation varied inversely with temperature (Table 1, Figs. 2–4, Supplementary Figs. 6–7). However, temperature is likely not the only factor contributing to some of these aspects of behavior as indicated by differential irrigation patterns and redox dynamics at in-situ temperatures with sediment and worms collected in winter compared to sediments and worms collected in summer and transitioned to wintertime temperatures.

### 4.2.1. Temporal patterns

Pumping and resting durations both increased with decreasing temperature during the temperature ramp experiment and were  $\sim$ 4

times longer at 5 °C than at 21 °C (Table 1, Fig. 2). A similar difference in irrigation patterns was observed in intact sediment cores collected in a dense maldanid bed in summer and winter (Table 1, Fig. 2). The combination of shorter pumping and resting events at higher temperatures results in an overall higher frequency of irrigation events at warmer temperatures. This finding is consistent with the idea that higher temperatures increase animal metabolic rates, feeding activity, and burrowing activity, increasing the demand for oxygen and necessitating more frequent burrow irrigation (Przesławski et al., 2009). Lower oxygen concentrations in overlying water at higher temperatures and a faster buildup of metabolites in the burrow resulting from the increased metabolic rate of the animal and/or the surrounding microbial community may further promote the more frequent burrow flushing at higher temperatures.

Throughout the downward temperature ramp in Experiment 2, pumping and resting durations increased at approximately the same rate, resulting in a relatively constant duty cycle of  $\sim\!50\%$  at all temperatures, and the animals in Experiment 1 (summer-collected) also pumped with a  $\sim\!50\%$  duty cycle (Table 1, Fig. 3C). Maldanids in the summer cores in Experiment 3B also pumped  $\sim\!50\%$  of the time, but contrary to the results of Experiment 2, animals in the winter cores in Experiment 3A only pumped  $\sim\!20\!-\!30\%$  of the time (Table 1, Fig. 2), displaying both shorter pumping durations and longer resting durations at 6 °C than the animals in the temperature ramp at 5 °C. Season-specific sediment characteristics, such as the supply of labile organic carbon, microbial activity, and the long-term acclimation of maldanids to season-specific conditions may therefore be important additional factors that govern irrigation patterns in maldanids.

Irrigation activity patterns of maldanids in intact cores collected in winter were significantly different from all other experiments. Specifically, duty cycles were significantly lower, and the pumping frequencies were significantly lower in intact winter cores than in sediment collected in summer and then cooled to winter temperatures (Fig. 2 and Fig. 5, respectively). It is well established that microbial and infaunal respiration increase with temperature, which was indeed reflected in the decline of oxygen consumption rates with temperatures in Experiment 2. The faster depletion of oxygen may then trigger more frequent irrigation with higher duty cycles in summer to sustain aerobic metabolism in maldanids. However, the fact that duty cycles were not significantly different between different temperatures in Experiment 2 suggests that other factors may play a role. Oxygen consumption rates estimated within feeding pockets in intact cores were not significantly different between summer and winter, likely due to the establishment of more oxidized conditions in frequently oxygenated sediment regions (Forster, 1996). The lower duty cycle of bioirrigation in intact cores collected in winter sediments suggests that, in permeable sediments, irrigation not only fulfills the role of supplying oxygen for infaunal respiration, but also the removal of toxic metabolic products of the worm such as nitrogenous wastes or products of anaerobic microbial respiration such as H<sub>2</sub>S. The production and accumulation of such products are generally known to be less pronounced in winter, which may not have been adequately mimicked in summer-collected sediments cooled to winter temperatures. In addition, Fuller (1994) showed that Clymenella is adversely affected by porewater H2S in summer months, while potentially developing a tolerance to it in the fall. Thus, acclimation to seasonspecific conditions may further affect irrigation activity patterns in maldanids.

# 4.2.2. Spatial patterns

*C. torquata* in our experiments tended to burrow deeper under colder conditions (Figs. 3–4). There are many potential explanations for this, but some of them can be ruled out as direct causes by this study. As previously mentioned, it has been found that high concentrations of porewater H<sub>2</sub>S in the 1–2 mM range can have adverse effects on *C. torquata*—especially in the summer—while they potentially acclimate and develop a greater tolerance during fall months (Fuller, 1994). In

incubation experiments using sediment from the Ponquogue site, porewater H<sub>2</sub>S concentrations of up to ~1.5 mM at depth were measured in the summer while H<sub>2</sub>S was not detectable in winter (Swenson Perger et al., 2023). This finding is expected given the higher temperatures, increased labile organic carbon inputs, and enhanced microbial metabolism in summer. H2S at depth, therefore, could have discouraged maldanids from burrowing deeper. However, it is unlikely that H<sub>2</sub>S concentrations in the antfarm during the temperature ramp changed immediately in response to the temperature change, and yet deeper activity was observed within 8 h after the temperature decline. In addition, the data presented here suggest that maldanids are quite effective in displacing reduced porewater, as oxic water frequently penetrated at least 4 mm away from each burrow's blind end during pumping in summer, and much farther (centimeters) in winter. To some extent, the shallow irrigation in intact summer cores may have been related to higher abundances of juvenile maldanids at the time of sampling. However, deep irrigation was rarely detected in any of the cores despite adult abundances between 412 and 657 individuals/m<sup>2</sup>. In addition, the transition from shallower to deeper irrigation by adult maldanids was observed with declining temperatures during the downward temperature ramp.

A similar response in burrowing depth to temperature changes has been observed in the nereid polychaete, Nereis diversicolor, including a rapid deepening of burrows in response to a sudden temperature drop (Esselink and Zwarts, 1989). Temperature itself was concluded to be the driving factor of burrowing depth in that case, suggesting that benthic organisms exposed to cold temperatures may be seeking thermal refugia deeper in the sediment (Esselink and Zwarts, 1989). This seasonal thermal refuge-seeking behavior by endobenthic organisms has also been observed in the burrowing mantis shrimp, Squilla empusa (Myers, 1979). In this context, it should be noted that no vertical temperature gradient was established in our experiments, since the goal was to establish general summertime and wintertime conditions rather than differential sediment surface heating or cooling. Still, the data suggest that irrigation depth changes in maldanids are a simple case of stimulus (low temperature) and response (switching to deep activity), as this behavioral change occurs in the absence of other changes in water or sediment characteristics.

Literature values for the burrowing depth of *C. torquata* are in the 10-30 cm range (Mangum, 1964; Rhoads, 1967; Fuller, 1994; Zorn et al., 2006), and predictions of their annual sediment reworking potential assume that this depth is relatively constant throughout the year. Our data, however, suggest that the activities of this polychaete may be much more concentrated in the upper 10 cm of the sediment column in warmer conditions and deepen once temperatures drop below ~12–15 °C. Likely, this threshold varies geographically, along the latitudinal distribution of C. torquata. There may also be a point at which the relationship between temperature and burrowing depth reverses when an upper temperature tolerance is approached, though a 50% lethal temperature of 38  $^{\circ}\text{C}$  has been reported for C. torquata if they are acclimated to warm temperatures (Kenny, 1969). As a result of seasonal dynamics in mixing depth, it is possible that some estimates of deep sediment turnover by C. torquata (and perhaps by other bioturbators, as noted above) are overestimated while shallow sediment turnover may be underestimated. This burrowing depth pattern also suggests that there may be seasonal variation in the mineralogy of particles transported to the sediment-water interface via maldanid feeding and defecation.

The data presented here further indicate a strong difference in oxygen penetration around maldanid tubes and around the feeding pockets. Zorn et al. (2006) suggested that oxygen penetrating through *Clymenella* (species unspecified) burrow walls is fully depleted within 0.3 mm of distance from the burrow. Especially at low temperatures, the images captured in our experiments clearly show that oxygen can penetrate further than 1 mm from tube walls and that these (still relatively thin) zones generally oscillate as rapidly or more rapidly than feeding pockets

in terms of redox conditions (Figs. 5–8, Supplementary Figs. 4–5). This penetration is presumably diffusive in nature and can be observed in tubes that both are and are not touching the aquarium's front plate, indicating that this is not an artifact of aquarium geometry. Burrow walls and adjacent sediment may consequently be greatly enriched in intermediate products of redox processes such as redox-active metastable minerals and may thus, despite the relatively small volume of sediment affected, be particularly important hot-spots for biologically-mediated redox reactions (Aller and Aller, 1986; Kristensen and Kostka, 2005; Gilbert et al., 2016).

# 4.3. Seasonal bioirrigation patterns and consequences for sedimentary redox dynamics

The stability of redox conditions created by differing bioturbation behavioral patterns varies seasonally (Fig. 5, Supplementary Data: SeasonalComparison.mp4). In winter conditions, feeding pockets remained oxic at their centers for relatively long-time intervals due low oxygen consumption, extended periods of active pumping and higher starting oxygen concentrations. Under these conditions, only the edges of the pockets switched between oxic and anoxic conditions in an actively ventilated burrow, while most of the feeding pocket remained oxic through the entire irrigation-rest cycle. By contrast, in summer conditions, feeding pockets frequently switched between oxic and anoxic throughout their volumes, resulting in dynamic redox conditions throughout the affected volume. A similar phenomenon was reported for three species of tellinid bivalves that inject water through their subsurface exhalant siphons (Volkenborn et al., 2012a). Frequent short pumping and resting intervals in the smallest of the three species (Macoma balthica) did not allow for oxygen depletion during resting intervals resulting in more sustained oxygenation than in the larger tellinids with longer irrigation and resting intervals (Volkenborn et al., 2012a). Likewise, oxygen presence in sediments around burrows of arenicolid polychaetes and thalassinid shrimp can be more stable in sandy sediment with low O2 demand, whereas rapid oscillations occurred in muddy sediment where O2 was rapidly consumed (Volkenborn et al., 2010; Volkenborn et al., 2012b). This study demonstrates that seasonal changes in irrigation patterns produce more stable geochemical conditions in winter when compared to rapidly oscillating conditions during summer.

More frequent oscillations in summer were generally accompanied by shorter oxic event durations than in winter sediments, and this was generally true in different sediment zones (Figs. 5, 6A-B). The distributions of redox oscillation rates, oxic event durations, and oxic probabilities in intermittently-oxic sediment were all heavily right-skewed, indicating that, while oxygenation is usually rare and short-lived, some oxygenation events occur more frequently and/or last orders of magnitude longer than others, consistent with the observation in North Sea sediments by Forster (1996). Although distributions varied, typical pumping and resting durations can be used to predict the most typical combined expressions of these redox characteristics in intermittently oxic sediments as described in section 2.2 (Figs. 7, 8). Conditions near the sediment-water interface were not always predictable in this way (Fig. 7B) and at times seemed to paradoxically display both high oscillation frequencies and long oxic event durations (Figs. 7, 8), likely because—unlike tubes or pockets, which are generally only influenced by a single individual—the movement of the oxic-anoxic boundary near the sediment-water interface is influenced by multiple animals simultaneously and is less likely to be the product of the behavior of a single individual. The threshold for "oxic conditions" was set at 10% saturation in order to exclude noise, but oxygen concentrations in summer feeding pockets often rose to near this threshold without exceeding it or only briefly exceeding it during a pumping event, and this may explain the disparity between pumping-pattern-based predictions and redox characteristics in these zones (Figs. 7E, 8E).

Since summer spatio-temporal irrigation patterns result in the

frequent but intermittent oxygenation of shallow sediments, especially those shallower than  $\sim 10$  cm, with  $\sim 25-100\%$  of bulk sediment at most depths in this range experiencing at least some oxygen exposure over the course of 6.2 days (Fig. 4B), reduced end products of redox pathways, such as hydrogen sulfide are likely quickly reoxidized to intermediate sulfur species and sulfate in the bioturbated zone (Thamdrup et al., 1994a; Thamdrup et al., 1994b; Jørgensen et al., 2019), but the lack of deeper bioadvection may result in higher H2S build-up and more reducing conditions deep in the sediment, potentially allowing sulfide to be sequestered as solid phase pyrite below  $\sim 10$  cm depth. Nonetheless, summer irrigation may enhance the release of a range of dissolved species, including N2O, Mn2+, and Fe2+ to the water column, as denitrification, dissimilatory manganese reduction, and dissimilatory iron reduction generally occur directly around burrows and in the upper several centimeters of the sediment column, and summer bioadvection has pronounced impacts at these depths (Gilbert et al., 2016; Peiffer et al., 2021). Pyrite oxidation and the subsequent release of oxidation products may also be enhanced by frequent redox oscillations. Pyrite framboid oxidation in carbonate-buffered solutions may follow a shrinking core model in which the oxidation rate is limited by the passivation of the framboid's surface layer resulting from the formation of an iron oxide coating (Nicholson et al., 1990), and Morse (1991) reports oxidation kinetics of pyrite in seawater that suggest this mechanism does indeed operate in marine sediments, with pyrite persisting for months in fully oxic seawater despite the initial 3-18% of oxidation occurring within the first day of exposure and an additional 20% occurring within the first week. Switching frequently between oxidizing and reducing conditions would allow for the periodic re-reduction and enhanced dissolution of this surface oxide layer, keeping oxidation rates maximal during periods of oxygen exposure, and potentially allowing pyrite oxidation to occur much faster than under continuously-oxic conditions. Finally, the overall less stable redox conditions in summer may result in the enrichment of redox-active metastable minerals—such as magnetite and humic acids-and reactive oxygen species-such as hydroxyl radical and hydrogen peroxide—in the bioturbated zone, which may help maintain exceptionally high rates of microbiallymediated redox processes in the case of the former, but may act to inhibit the microbial community in the case of the latter (Trusiak et al., 2018; Peiffer et al., 2021).

In winter, by contrast, more stable redox conditions resulting from less frequent pumping and resting as well as persistence of oxygen in feeding pockets between pumping events likely allow for denitrification to proceed all the way to N<sub>2</sub>, and the higher availability of oxygen allows for dissolved species, including Mn2+ and Fe2+ to be re-oxidized and precipitated in mineral forms before they can be released, which would result in lower benthic metal fluxes. Pyrite framboids in these zones would likely build up thick surface oxide layers, passivating their surfaces and slowing their oxidation rates in the long term, although enhanced pyrite oxidation may still occur in the oscillatory zones on the outer edges of feeding pockets. In zones that remain anoxic for extended periods of time, hydrogen sulfide produced during sulfate reduction likely reacts with dissolved and solid phase iron to eventually form pyrite (Berner, 1984). Generally speaking, these conditions would result in more stable mineralogy and lower fluxes of most elements, though iron monosulfide production may be high in oscillatory zones around pockets, where high rates of iron oxidation may be coupled with intermittent exposure to high concentrations of hydrogen sulfide.

# 5. Conclusions

Changing temperature alone is not an adequate substitute for conducting experiments in-season at field temperatures. Maldanids did not display the same overall behavior in summer sediments cooled to winter temperatures as they displayed in winter sediments. Thus, the geochemical expression of infaunal activity in response to an artificial temperature change differs from the normal seasonal behavior. Seasonal

factors beyond temperature must be responsible for these differences. The simplest way to avoid experimental artifacts and uncertainties is to work in-season.

The data presented here can help to parameterize future work with bioirrigation mimics or geochemical reaction-transport models. Temperature can be used to roughly estimate the expected pumping interval length at a selected experimental temperature, and a duty cycle between  $\sim\!50\%$  and  $\sim\!25\%$  (erring lower at lower temperatures) can be used to predict the resting interval length. Using literature values for bioirrigation volumes (Mangum, 1964), it is then possible to estimate the volume that must be pumped during each of these intervals to mimic one or several individuals.

Bioirrigation depth can also be parameterized based on temperature. The maldanid polychaete C. torquata primarily irrigates within the top  $\sim\!10$  cm of the sediment column at temperatures warmer than  $\sim\!19$  °C, while at temperatures  $\sim\!15$  °C and below, they introduce oxic water down to at least  $\sim\!20$  cm depth in the sediment column with comparably less activity near the sediment surface.

Finally, the typical oxygen dynamics induced by a given bioirrigator pumping/resting pattern in intermittently-oxic sediment can be predicted fairly accurately from pumping and resting durations. Because this relationship is presumably not species-specific, it may be used broadly to inform and simplify the parameterization of reaction-transport models that improve our understanding of biogeochemical processes and solute transport in bioturbated permeable sediments.

Supplementary data to this article can be found online at https://doi. org/10.1016/j.jembe.2024.151987.

#### **Author statement**

IPD: Conceptualization, Methodology, Software, Validation, Formal analysis, Investigation, Data Curation, Writing - Original Draft, Writing - Review & Editing, Visualization

DAS: Investigation, Resources, Writing - Review & Editing

MG: Methodology, Investigation, Data Curation, Formal analysis

RCA: Conceptualization, Writing - Review & Editing, Resources, Supervision, Project administration, Funding acquisition

LMW Writing - Review & Editing, Supervision, Resources, Project administration, Funding acquisition

NV: Conceptualization, Methodology, Software, Validation, Formal analysis, Investigation, Resources, Data Curation, Writing - Original Draft, Writing - Review & Editing, Visualization, Supervision, Project administration. Funding acquisition

#### **Funding**

This project was funded by the National Science Foundation (OCE-1757045); and by a SBU Presidential Dissertation Completion Award to L.P.D.

### CRediT authorship contribution statement

Ian P. Dwyer: Conceptualization, Data curation, Formal analysis, Investigation, Methodology, Software, Validation, Visualization, Writing – original draft, Writing – review & editing. Darci A. Swenson Perger: Investigation, Resources, Writing – review & editing. Molly Graffam: Data curation, Investigation, Methodology, Writing – review & editing. Robert C. Aller: Conceptualization, Funding acquisition, Project administration, Resources, Supervision, Writing – review & editing. Laura M. Wehrmann: Funding acquisition, Project administration, Supervision, Writing – review & editing. Nils Volkenborn: Conceptualization, Data curation, Formal analysis, Funding acquisition, Investigation, Methodology, Resources, Project administration, Software, Supervision, Validation, Visualization, Writing – original draft, Writing – review & editing.

#### Declaration of competing interest

The authors declare the following financial interests/personal relationships which may be considered as potential competing interests:

Ian P. Dwyer reports financial support was provided by National Science Foundation. Darci A. Swenson Perger reports financial support was provided by National Science Foundation. Nils Volkenborn reports financial support was provided by National Science Foundation. Robert C. Aller reports financial support was provided by National Science Foundation. Laura M. Wehrmann reports was provided by National Science Foundation. Ian P. Dwyer reports financial support was provided by Stony Brook University.

#### Data availability

Data will be made available on request.

# Acknowledgments

We want to acknowledge Lubos Polerecky's leading role in the development of the planar optode imaging technique and related data acquisition/processing tools to advance bioturbation research that informed and inspired our study. We would also like to thank Sarah Ann Woodin and David S. Wethey for helping with porewater pressure measurement instrumentation and letting us use their oxygen optode imaging equipment. Stefan Forster and one anonymous reviewer are thanked for thoughtful and constructive comments that helped to improve the manuscript.

#### References

- Aller, R.C., 1994. Bioturbation and remineralization of sedimentary organic matter: effects of redox oscillation. Chem. Geol. 114, 331–345. https://doi.org/10.1016/ 0009-2541(94)90062-0.
- Aller, R.C., 2014. Sedimentary diagenesis, depositional environments, and benthic fluxes. In: Turekian, K., Holland, H. (Eds.), Treatise on Geochemistry, 2nd edition, pp. 293–334.
- Aller, R.C., Aller, J.Y., 1986. Evidence for localized enhancement of biological activity associated with tube and burrow structures in deep-sea sediments at the HEEBLE site, western North Atlantic. Deep Sea Res. Part I Oceanogr. 33, 775–790. https:// doi.org/10.1016/0198-0149(86)90088-9.
- Aller, R.C., Aller, J.Y., 1998. The effect of biogenic irrigation intensity and solute exchange on diagenetic reaction rates in marine sediments. J. Mar. Res. 56, 905–936. https://doi.org/10.1357/002224098321667413.
- Banta, G.T., Holmer, M., Jensen, M.H., Kristensen, E., 1999. Effects of two polychaete worms, *Nereis diversicolor* and *Arenicola marina*, on aerobic and anaerobic decomposition in a sandy marine sediment. Aquat. Microb. Ecol. 19, 189–204. https://doi.org/10.3354/ame019189.
- Berner, R.A., 1984. Sedimentary pyrite formation: an update. Geochim. Cosmochim. 48, 605–615. https://doi.org/10.1016/0016-7037(84)90089-9.
- Blair, N.E., Aller, R.C., 2012. The fate of terrestrial organic carbon in the marine environment. Ann. Rev. Mar. Sci. 4, 401–423. https://doi.org/10.1146/annurevmarine-120709-142717.
- Burdige, D.J., 2011. Estuarine and coastal sediments coupled biogeochemical cycling. In: Wolanski, E., McLusky, D. (Eds.), Treatise on Estuarine and Coastal Science, Biogeochemistry, Vol 5. Academic Press, pp. 279–316.
- Cai, W.J., 2011. Estuarine and coastal ocean carbon paradox: CO<sub>2</sub> sinks or sites of terrestrial carbon incineration? Ann. Rev. Mar. Sci. 3, 123–145. https://doi.org/ 10.1146/annurev-marine-120709-142723.
- Dobbs, F.C., Whitlatch, R.B., 1982. Aspects of deposit-feeding by the polychaete Clymenella torquata. Ophelia. 21, 159–166. https://doi.org/10.1080/ 00785326.1982.10426584.
- Esselink, P., Zwarts, L., 1989. Seasonal trend in burrow depth and tidal variation in feeding activity of *Nereis diversicolor*. Mar. Ecol. Prog. Ser. 56, 243–254. https://doi. org/10.3354/meps056243.
- Forster, S., 1996. Spatial and temporal distribution of oxidation events occurring below the sediment-water interface. Mar. Ecol. 17, 309–319. https://doi.org/10.1111/ i.1439-0485.1996.tb00510.x.
- Forster, S., Graf, G., 1995. Impact of irrigation on oxygen flux into the sediment: intermittent pumping by *Callianassa subterranea* and "piston-pumping" by *Lanice conchilega*. Mar. Biol. 123, 335–346. https://doi.org/10.1007/BF00353625.
- Fuller, C.M., 1994. Effects of porewater hydrogen sulfide on the feeding activity of the subsurface deposit-feeding polychaete, Clymenella torquata, Leidy. J. Mar. Res. 52, 1101–1127. https://doi.org/10.1357/0022240943076821.
- Gilbert, F., Hulth, S., Grossi, V., Aller, R.C., 2016. Redox oscillation and benthic nitrogen mineralization within burrowed sediments: an experimental simulation at low frequency. J. Exp. Mar. Biol. Ecol. 482, 75–84.

- Hölker, F., Vanni, M.J., Kuiper, J.J., Meile, C., Grossart, H.P., Stief, P., Adrian, R., Lorke, A., Dellwig, O., Brand, A., Hupfer, M., Mooij, W.M., Nützmann, G., Lewandowski, J., 2015. Tube-dwelling invertebrates: tiny ecosystem engineers have large effects in lake ecosystems. Ecol. Monogr. 85, 333–351. https://doi.org/10.1890/14-1160.1.
- Holst, G., Grunwald, B., 2001. Luminescence lifetime imaging with transparent oxygen optodes. Sens. Actuators B Chem. 74, 78–90. https://doi.org/10.1016/S0925-4005 (00)00715-2
- Holst, G., Kohls, O., Klimant, I., König, B., Kühl, M., Richter, T., 1998. A modular luminescence lifetime imaging system for mapping oxygen distribution in biological samples. Sens. Actuators B Chem. 51, 163–170. https://doi.org/10.1016/S0925-4005(98)00232-9.
- Jørgensen, B.B., Revsbech, N.P., 1985. Diffusive boundary layers and the oxygen uptake of sediments and detritus. Limnol. Oceanogr. 30, 111–122.
- Jørgensen, B.B., Findlay, A.J., Pellerin, A., 2019. The biogeochemical sulfur cycle of marine sediments. Front. Microbiol. 10, 849. https://doi.org/10.3389/ fmicb.2019.00849.
- Kenny, R., 1969. Temperature tolerance of the polychaete worms Diopatra cuprea and Clymenella torquata. Mar. Biol. 4, 219–223. https://doi.org/10.1007/BF00393896.
- Kristensen, E., Kostka, J.E., 2005. Macrofaunal burrows and irrigation in marine sediment: microbiological and biogeochemical interactions. In: Kristensen, E.,
   Haese, R.R., Kostka, J.E. (Eds.), Interactions Between Macro- and Microorganisms in Marine Sediments 60. American Geophysical Union, Washington, D. C, pp. 125–157.
- Levin, L., Blair, N., DeMaster, D., Plaia, G., Fornes, W., Martin, C., Thomas, C., 1997.
  Rapid subduction of organic matter by maldanid polychaetes on the North Carolina slope. J. Mar. Res. 55, 595–611. https://doi.org/10.1357/0022240973224337.
- Liu, K.K., Atkinson, L., Quiñones, R., Talaue-McManus, L., 2010. Carbon and Nutrient Fluxes in Continental Margins: A Global Synthesis. Springer Science & Business Media, Berlin/Heidelberg, Germany.
- Mach, M.E., Levings, C.D., McDonald, P.S., Chan, K.M., 2012. An Atlantic infaunal engineer is established in the northeast Pacific: Clymenella torquata (Polychaeta: Maldanidae) on the British Columbia and Washington Coasts. Biol. Invasions 14, 503–507. https://doi.org/10.1007/s10530-011-0096-6.
- Mangum, C.P., 1964. Activity patterns in metabolism and ecology of polychaetes. Comp. Biochem. Physiol. 11, 239–256. https://doi.org/10.1016/0010-406X(64)90105-7.
- Matsui, G.Y., Volkenborn, N., Polerecky, L., Henne, U., Wethey, D.S., Lovell, C.R., Woodin, S.A., 2011. Mechanical imitation of bidirectional bioadvection in aquatic sediments. Limnol. Oceanogr.: Methods. 9, 84–96. https://doi.org/10.4319/ lom.2011.9.84.
- Meysman, F.J., Middelburg, J.J., Heip, C.H., 2006. Bioturbation: a fresh look at Darwin's last idea. Trends Ecol. Evol. 21, 688–695. https://doi.org/10.1016/j. tree.2006.08.002.
- Morse, J.W., 1991. Oxidation kinetics of sedimentary pyrite in seawater. Geochim. Cosmochim. Acta 55, 3665–3667. https://doi.org/10.1016/0016-7037(91)90064-C.
- Myers, A.C., 1979. Summer and winter burrows of a mantis shrimp, Squilla empusa, in Narragansett Bay, Rhode Island (USA). Estuar. Coast. Mar. Sci. 8, 87–98. https://doi. org/10.1016/0302-3524(79)90107-5.
- Nicholson, R.V., Gillham, R.W., Reardon, E.J., 1990. Pyrite oxidation in carbonate-buffered solution 2: rate control by oxide coatings. Geochim. Cosmochim. Acta 54, 395–402. https://doi.org/10.1016/0016-7037(90)90328-I.
- Peiffer, S., Kappler, A., Haderlein, S.B., Schmidt, C., Byrne, J.M., Kleindienst, S., Vogt, C., Richnow, H.H., Obst, M., Angenent, L.T., Bryce, C., McCammon, C., Planer-Friedrich, B., 2021. A biogeochemical-hydrological framework for the role of redoxactive compounds in aquatic systems. Nat. Geosci. 14, 264–272. https://doi.org/ 10.1038/s41561-021-00742-z.
- Polerecky, L., Franke, U., Werner, U., Grunwald, B., de Beer, D., 2005. High spatial resolution measurement of oxygen consumption rates in permeable sediments. Limnol. Oceanogr. Methods 3, 75–85. https://doi.org/10.4319/lom.2005.3.75.
- Polerecky, L., Volkenborn, N., Stief, P., 2006. High temporal resolution oxygen imaging in bioirrigated sediments. Environ. Sci. Technol. 40, 5763–5769. https://doi.org/ 10.1021/es0604941.
- Precht, E., Franke, U., Polerecky, L., Huettel, M., 2004. Oxygen dynamics in permeable sediments with wave-driven pore water exchange. Limnol. Oceanogr. 49, 693–705.
- Przeslawski, R., Zhu, Q., Aller, R., 2009. Effects of abiotic stressors on infaunal burrowing and associated sediment characteristics. Mar. Ecol. Prog. Ser. 392, 33–42. https://doi.org/10.3354/meps08221.
- Rhoads, D.C., 1967. Biogenic reworking of intertidal and subtidal sediments in Barnstable Harbor and Buzzards Bay, Massachusetts. J. Geol. 75, 461–476. https://doi.org/10.1086/627272.
- Sanders, H.L., Goudsmit, E.M., Mills, E.L., Hampson, G.E., 1962. A study of the intertidal fauna of Barnstable Harbor, Massachusetts 1. Limnol. Oceanogr. 7, 63–79. https:// doi.org/10.4319/10.1962.7.1.0063.
- Swenson Perger, D.A., Dwyer, I.P., Aller, R.C., Volkenborn, N., Heilbrun, C., Wehrmann, L.M., 2023. Seasonal iron fluxes and iron cycling in sandy bioirrigated sediments. Front. Mar. Sci. 10, 1293893. https://doi.org/10.3389/ fmars 2023.193883
- Thamdrup, B., Finster, K., Fossing, H., Hansen, J.W., Jørgensen, B.B., 1994a. Thiosulfate and sulfite distributions in porewater of marine sediments related to manganese, iron, and sulfur geochemistry. Geochim. Cosmochim. 58, 67–73. https://doi.org/ 10.1016/0016-7037(94)90446-4.
- Thamdrup, B., Fossing, H., Jørgensen, B.B., 1994b. Manganese, iron, and sulfur cycling in a coastal marine sediment, Aarhus Bay, Denmark. Geochem. Cosmochim. 23, 5115–5129. https://doi.org/10.1016/0016-7037(94)90298-4.
- Thomas, H., Schiettecatte, L.S., Suykens, K., Koné, Y.J.M., Shadwick, E.H., Prowe, A.E.F., Bozec, Y., de Baar, H.J.W., Borges, A.V., 2009. Enhanced ocean carbon storage from

- anaerobic alkalinity generation in coastal sediments. Biogeosciences. 6, 267–274. https://doi.org/10.5194/bg-6-267-2009.
- Trusiak, A., Treibergs, L.A., Kling, G.W., Cory, R.M., 2018. The role of iron and reactive oxygen species in the production of  $CO_2$  in arctic soil waters. Geochim. Cosmochim. Acta 224, 80–95. https://doi.org/10.1016/j.gca.2017.12.022.
- van de Velde, S., Meysman, F.J., 2016. The influence of bioturbation on iron and sulphur cycling in marine sediments: a model analysis. Aquat. Geochem. 22, 469–504. https://doi.org/10.1007/s10498-016-9301-7.
- Venables, W.N., Ripley, B.D., 2002. Modern Applied Statistics with S, fourth ed. Springer, New York.
- Volkenborn, N., Polerecky, L., Wethey, D.S., Woodin, S.A., 2010. Oscillatory porewater bioadvection in marine sediments induced by hydraulic activities of *Arenicola marina*. Limnol. Oceanogr. 55, 1231–1247. https://doi.org/10.4319/ lo.2010.55.3.1231.
- Volkenborn, N., Meile, C., Polerecky, L., Wethey, D.S., Woodin, S.A., Pilditch, C.A., Norkko, A., Norkko, J., Hewitt, J.E., Thrush, S.F., 2012a. Intermittent bioirrigation and oxygen dynamics in permeable sediments: an experimental and modeling study of three tellinid bivalves. J. Mar. Res. 70, 794–823. https://doi.org/10.1357/ 002224012806770955.

- Volkenborn, N., Polerecky, L., Wethey, D.S., DeWitt, T.H., Woodin, S.A., 2012b. Hydraulic activities by ghost shrimp *Neotrypaea californiensis* induce oxic-anoxic oscillations in sediments. Mar. Ecol. Prog. Ser. 455, 141–156. https://doi.org/10.3354/meps09645.
- Volkenborn, N., Woodin, S.A., Wethey, D.S., Polerecky, L., 2016. Bioirrigation in marine sediments. In: Reference Module in Earth Systems and Environmental Sciences. Elsevier Inc., pp. 1–9
- Wehrmann, L.M., Swenson Perger, D.A., Dwyer, I.P., Volkenborn, N., Heilbrun, C., Aller, R.C., 2023. Ideas and perspectives: the benthic iron flux from sandy advective bioturbated sediments. Biogeosci. Discuss. 1-21 https://doi.org/10.5194/bg-2022-247
- Wethey, D.S., Woodin, S.A., 2005. Infaunal hydraulics generate porewater pressure signals. Biol. Bull. 209, 139–145. https://doi.org/10.2307/3593131.
- Wickham, H., 2016. ggplot2: Elegant Graphics for Data Analysis. Springer-Verlag, New York.
- Zorn, M.E., Lalonde, S.V., Gingras, M.K., Pemberton, S.G., Konhauser, K.O., 2006. Microscale oxygen distribution in various invertebrate burrow walls. Geobiology. 4, 137–145. https://doi.org/10.1111/j.1472-4669.2006.00074.x.